AD-A137 435 TEMPERATURE EFFECTS OF CEMENT JOINTS IN CERAMIC-STACK RSSONATORS(U) NAVAL OCEAN SYSTEMS CENTER SAN DIEGO CA C L GOODHART JUN 8 NOSC/TR-860 1/1

UNCLASSIFIED F/G 9/1 NL

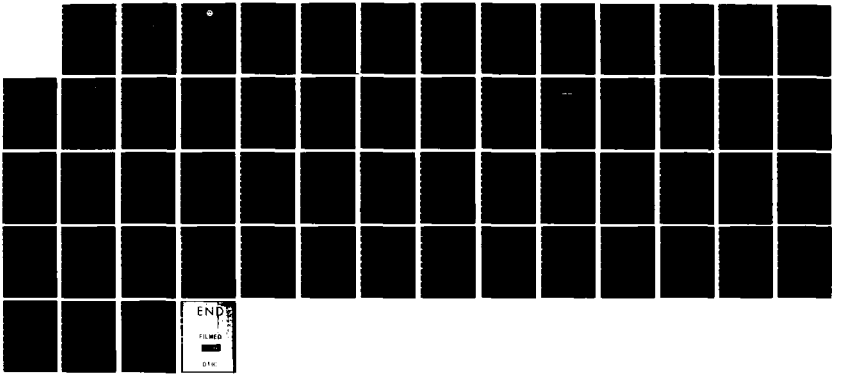

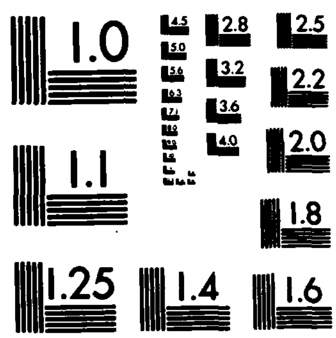

MICROCOPY RESOLUTION TEST CHART
NATIONAL BUREAU OF STANDARDS-1963-A

(12)

NOSC TR 860

AD A137435

NOSC TR 860

Technical Report 860

TEMPERATURE EFFECTS OF CEMENT JOINTS IN CERAMIC-STACK RESONATORS

C. L. Goodhart

June 1983
Final Report:
April 1982 — December 1982

Prepared for
Naval Research Laboratory/
Underwater Sound Reference Detachment
(NRL/USRD) Orlando, FL 32856

NOSC
NAVAL OCEAN SYSTEMS CENTER
San Diego, California 92152

NAVAL OCEAN SYSTEMS CENTER, SAN DIEGO, CA 92152

AN ACTIVITY OF THE NAVAL MATERIAL COMMAND

JM PATTON, CAPT, USN
Commander

HL BLOOD
Technical Director

ADMINISTRATIVE INFORMATION

The work reported herein was performed by the Sensors and Spatial Processing Division (Code 712) over the period April 1982 to December 1982. The work was supported by the Naval Research Laboratory/Underwater Sound Reference Detachment under project WS55712A, program element 24281N, subproject S1307-AS. This report completes a research effort initiated in October 1980.

Released by
T.F. Beeson, CDR, USN, Acting Head
Sensors and Spatial Processing
Division

Under authority of
H.A. Schenck, Head
Undersea Surveillance
Department

ACKNOWLEDGEMENTS

The author thanks H.H. Ding for his invaluable contributions to the computer modeling efforts and for many fruitful discussions. I am also grateful to Dr. G.E. Martin (Martin Acoustic Software Technology) for his technical expertise in providing the ceramic parameter determinations. I also thank Dr. G.W. Benthien and Dr. J.C. Lockwood for their valuable assistance and suggestions regarding this work. Appreciation is also expressed to D. Barach for his role in the modeling effort, to C.T. Bell, P.C. Bradshaw, J.J. Cross, and G. Gusman for their assistance in the experimental work, and to Dr. R.W. Timme (NRL) for sponsoring the work presented here.

UNCLASSIFIED

SECURITY CLASSIFICATION OF THIS PAGE *(When Data Entered)*

REPORT DOCUMENTATION PAGE

READ INSTRUCTIONS BEFORE COMPLETING FORM

1. REPORT NUMBER: NOSC Technical Report 860 (TR 860)	2. GOVT ACCESSION NO.: AD-A137 435
3. RECIPIENT'S CATALOG NUMBER:	
4. TITLE *(and Subtitle)*: TEMPERATURE EFFECTS OF CEMENT JOINTS IN CERAMIC-STACK RESONATORS	5. TYPE OF REPORT & PERIOD COVERED: Final Report, April 1982–December 1982
	6. PERFORMING ORG. REPORT NUMBER:
7. AUTHOR(s): CL Goodhart	8. CONTRACT OR GRANT NUMBER(s):
9. PERFORMING ORGANIZATION NAME AND ADDRESS: Naval Ocean Systems Center, San Diego CA 92152	10. PROGRAM ELEMENT, PROJECT, TASK AREA & WORK UNIT NUMBERS: 24281N, WS55712A, S1307-AS
11. CONTROLLING OFFICE NAME AND ADDRESS: Naval Research Laboratory/Underwater Sound Reference Detachment, Orlando FL 32856	12. REPORT DATE: June 1983
	13. NUMBER OF PAGES: 54
14. MONITORING AGENCY NAME & ADDRESS*(if different from Controlling Office)*:	15. SECURITY CLASS. *(of this report)*: Unclassified
	15a. DECLASSIFICATION/DOWNGRADING SCHEDULE:

16. DISTRIBUTION STATEMENT *(of this Report)*

Approved for public release, distribution unlimited

17. DISTRIBUTION STATEMENT *(of the abstract entered in Block 20, if different from Report)*

18. SUPPLEMENTARY NOTES

19. KEY WORDS *(Continue on reverse side if necessary and identify by block number)*

Transducers
Sonar
Piezoelectric ceramics
Ceramic-stack resonators
Cement joints
Epoxy joints

20. ABSTRACT *(Continue on reverse side if necessary and identify by block number)*

A temperature-related performance degradation has been observed in certain sonar transducers that employ ceramic-stack 33-mode resonators that contain cement joints. This study sought to identify the cause of this performance degradation and to determine resonator design or assembly methods that limit or eliminate this degradation. Experimental and computer modeling results show that the performance degradation is extreme for little or no final stress bias on the resonators and does not appear to be affected by the initial stress bias (the bias during cement curing). The degradation results from a temperature sensitivity of the stiffness of the cement/electrode joints. A high final stress bias of 2.8×10^7 Pa essentially eliminates the performance degradation.

DD FORM 1 JAN 73 1473 EDITION OF 1 NOV 65 IS OBSOLETE

S/N 0102-LF-014-6601

UNCLASSIFIED

SECURITY CLASSIFICATION OF THIS PAGE *(When Data Entered)*

CONTENTS

SUMMARY

PROBLEM

In November of 1978, a number of prototype sonar transducers were observed to exhibit current/thermal runaway when driven continuously with a constant-voltage source near the maximum designed drive level. Experimental tests indicated the source of the problem to be temperature-related performance degradation of the ceramic-stack resonators used in the transducers.

OBJECTIVES

The goals of this study were to:

- Understand the role of cement/electrode joints in the temperature sensitivity of ceramic-stack resonators.
- Understand, in turn, the mechanism by which the resonator temperature sensitivity causes current/thermal runaway.
- Determine resonator design or assembly techniques that limit or eliminate the temperature-related degradation.

RESULTS

Experimental and computer modeling results show that the temperature sensitivity of ceramic-stack resonators is related to a variation with temperature of the stiffness of the cement/electrode joints. The temperature sensitivity is only crucial in instances in which there is little or no final stress bias on the resonator and appears to be essentially independent of the initial stress bias (the bias during cement curing).

The current/thermal runaway phenomenon that was observed in certain sonar transducers results from the presence of ceramic-stack resonators that contain low final stress biases. The low stress bias allows self-heating to cause the joint stiffness to decrease as the temperature rises. The decreasing joint stiffness forces the impedance vs frequency responses of the resonators

to shift down in frequency, bringing lower impedance regions into the operation band, which was originally centered about an impedance maximum in the response curve. The resulting rise in current causes further heating leading to current/thermal runaway.

RECOMMENDATIONS

In order to eliminate the temperature-related performance degradation recently observed in sonar transducers, a high final stress-bias should be applied to the ceramic-stack resonators. A final stress bias of 2.8×10^7 Pa yields safe and consistent behavior and is presently being employed in the production of many ceramic-stack resonators.

1.0 BACKGROUND

1.1 DISCOVERY OF THE CURRENT/THERMAL RUNAWAY PHENOMENON

In November of 1978 a number of first-article sonar transducers were tested under the Composite-Unit Accelerated Life Testing (CUALT) program. The transducers employed piezoelectric ceramic-stack resonators (Figure 1) as the active elements. Such resonators contain piezoelectric-ceramic rings that are cemented* together to ensure good mechanical coupling and lateral strength between adjacent rings. Because the ceramic is weak in tension, the stress rod and nut (tail mass) provide a stress bias to keep the ceramic under compression. Nickel expanded-metal electrodes provide electrical connections between the rings. Figure 2 illustrates, in schematic form, the essential elements of the transducer. The oil-filled housing has a rubber window (not shown) for the transmission of the acoustic energy into the ocean. The drive is a constant-amplitude AC voltage source.

During the CUALT, some of the transducers exhibited current-runaway behavior when driven with the constant-voltage source near the maximum designed drive level. Figure 3 shows the actual current behavior for one of the transducers. Note that the current magnitude initially decreased a small amount, but eventually rose rather rapidly and dramatically. In addition, the current phase shows that the admittance changed monotonically from inductive to capacitive values. It was also noted in later experiments that a continual and significant temperature rise (at times reaching 115°C) accompanied this current behavior. Thus current/thermal runaway describes the phenomenon more accurately. When left unchecked, this runaway condition would result in transducer failure due to the effects of excessive heating.

*Actually, epoxy is used, but to conform with the usage of previous reports, epoxy will be referred to as cement in this report.

J = CEMENT/ELECTRODE JOINT
C = CERAMIC

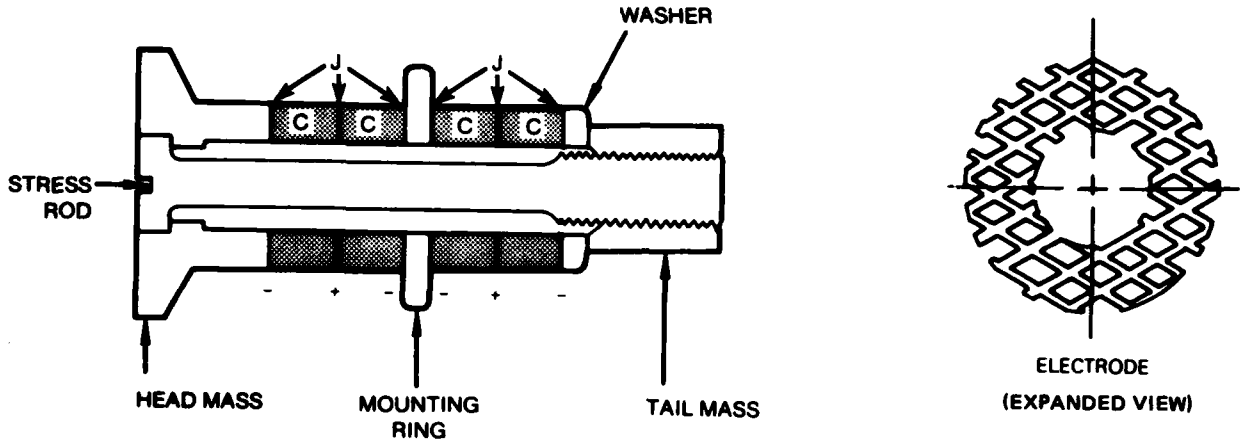

Figure 1. Piezoelectric ceramic-stack resonator.

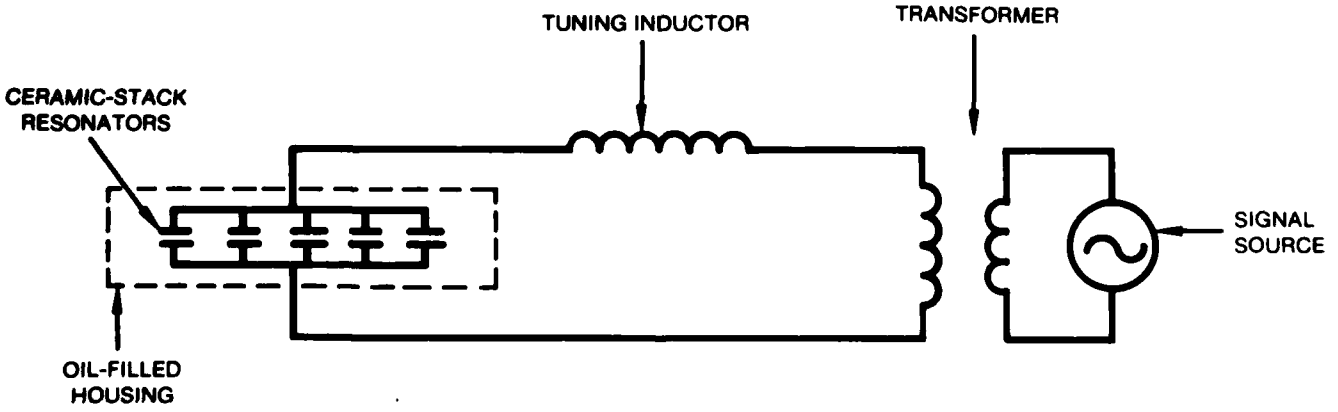

Figure 2. Underwater acoustic transducer.

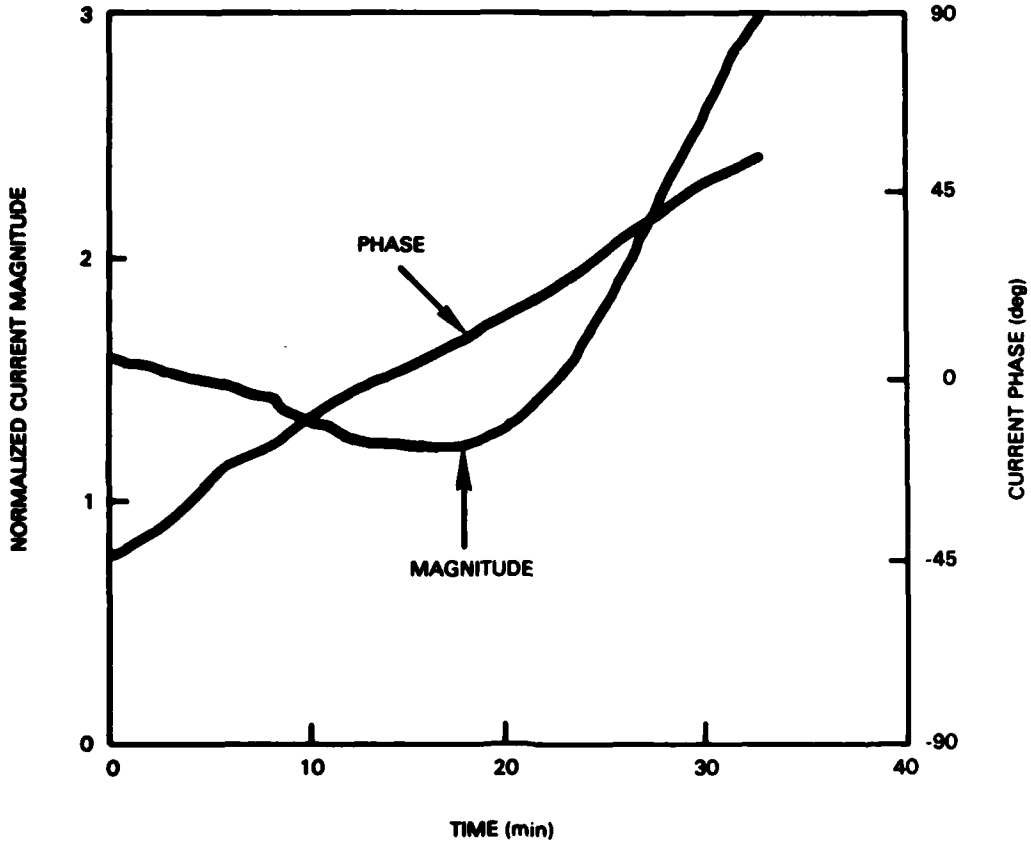

Figure 3. Current runaway phenomenon for an actual transducer.

1.2 DISCOVERY OF THE TEMPERATURE SENSITIVITY OF RESONATORS

A number of possible causes of the problem were investigated, with the final indication being that the current/thermal runaway was related to a temperature-dependent behavior of the resonators that were incorporated in the transducer. Some of the transducers were disassembled and the electrical input impedance vs frequency response of the individual resonators was examined in air at various temperatures. These measurements were made in a temperature-controlled oven by means of the method and equipment illustrated in Figure 4. The temperature in the oven was raised in increments of about 22°C and allowed to stabilize for at least 30 min after each increment. At each temperature, the electrical input impedance of each resonator was measured while it was being driven with a constant-amplitude, 10-V rms source that was swept in frequency over a range that included the operation band of

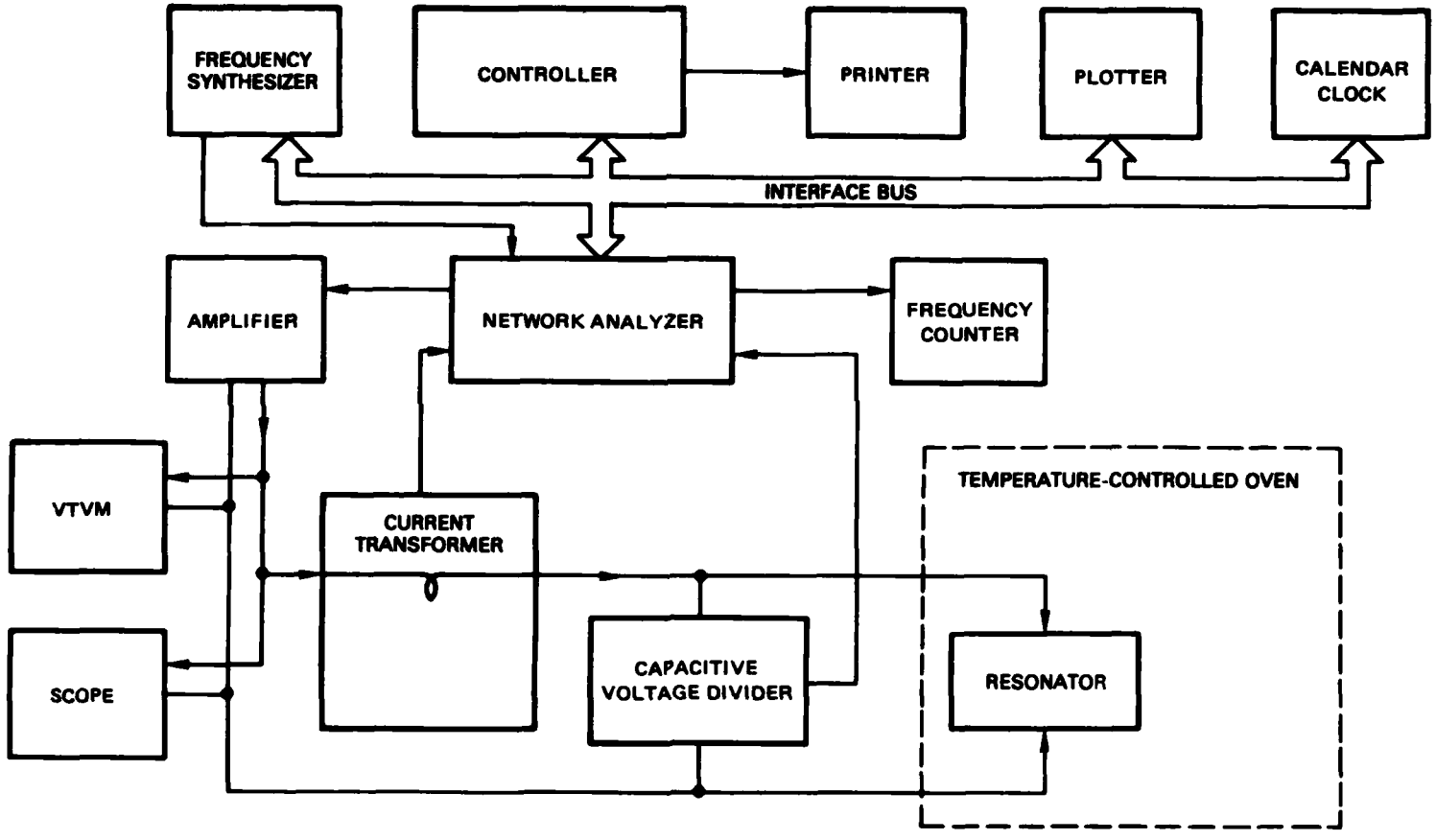

Figure 4. Block diagram of automated in-air impedance vs temperature measurements of ceramic-stack resonators.

the transducer. A typical result is shown in Figure 5. The frequency of minimum impedance magnitude, Z_m, is the resonant frequency, f_m, and the frequency of maximum impedance magnitude, Z_n, is the antiresonant frequency, f_n. The overall electromechanical coupling in a longitudinal resonator is generally proportional to $(f_n-f_m)/f_n = \Delta f/f_n$, while the overall resonator loss is inversely proportional to the impedance magnitude difference, $Z_n-Z_m = \Delta Z$. The above parameters are indicated for the 22°C curve in Figure 5. The larger the $\Delta f/f_n$ and ΔZ, the better the resonator. Figure 5 shows that the impedance vs frequency curve shifts down in frequency as the temperature rises. In addition, Δf and ΔZ decrease, indicating that the coupling decreases and the losses increase as the temperature rises; the resonator performance deteriorates with rising temperature. The resonator nearly recovers its original behavior when returned to room temperature (22°C). In a few of the resonators tested, the impedance magnitude vs frequency response at 121°C was markedly shifted down in frequency and was nearly flat, indicating severe degradation of the resonator performance (Figure 6).

Two of the transducers that had exhibited current runaway were subsequently disassembled, and each of the five resonators (per transducer) was tested for its temperature sensitivity, by means of in-air impedance measurements in the oven. Figure 7 shows results for the worst resonator in each transducer. In general, the other eight resonators behaved at least slightly better than resonator S-4871 (Figure 7a). During the CUALT, the transducer that contained resonator S-4871 (Figure 7a) was subjected to a 126-V rms drive, which caused the current to increase by a factor of 1.8 in about 45 min. For the transducer that contained resonator S-4853 (Figure 7b), a 110-V rms drive caused the current to increase by a factor of 2.5 in about 30 min. Clearly, the later transducer was more susceptible to current runaway. This susceptibility appears to be related to the marked temperature sensitivity of resonator S-4853 as evidenced by the in-air oven measurements.

A practical solution to the problem was found to be an increase in the initial and final stress biases* from 6.9×10^6 Pa (1000 psi) to 2.8×10^7 Pa

*An initial stress is applied prior to the cement cure, then a final stress is applied after the cure.

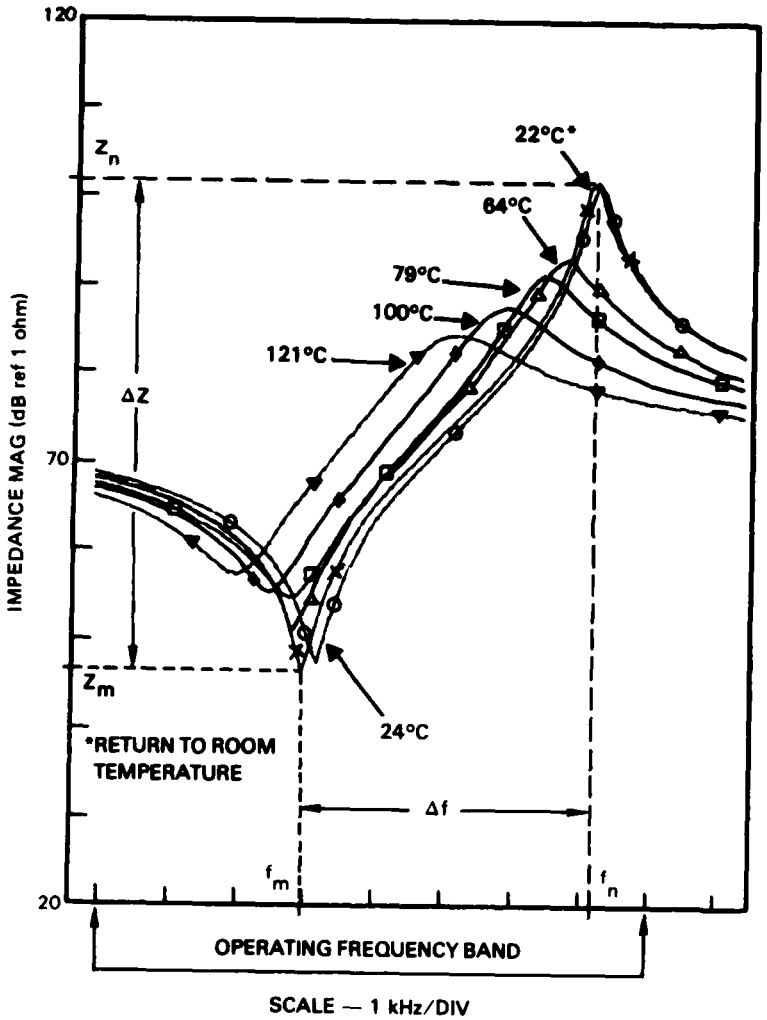

Figure 5. Measurements of impedance magnitude vs frequency for a ceramic-stack resonator in air at various temperatures.

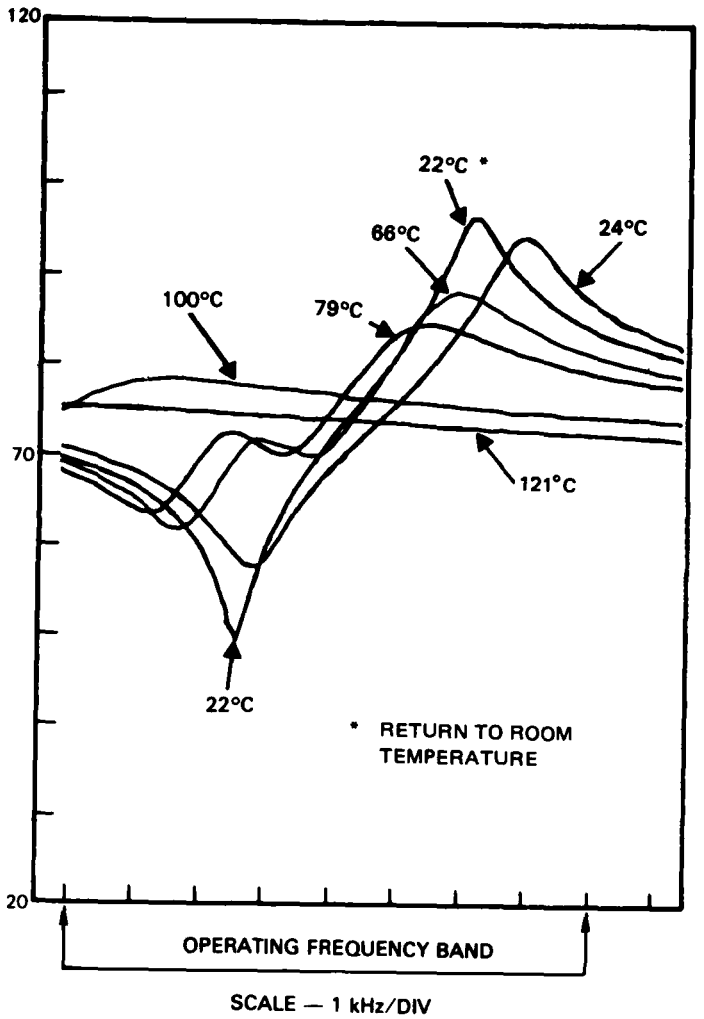

Figure 6. Oven measurements for a resonator that is extremely sensitive to temperature.

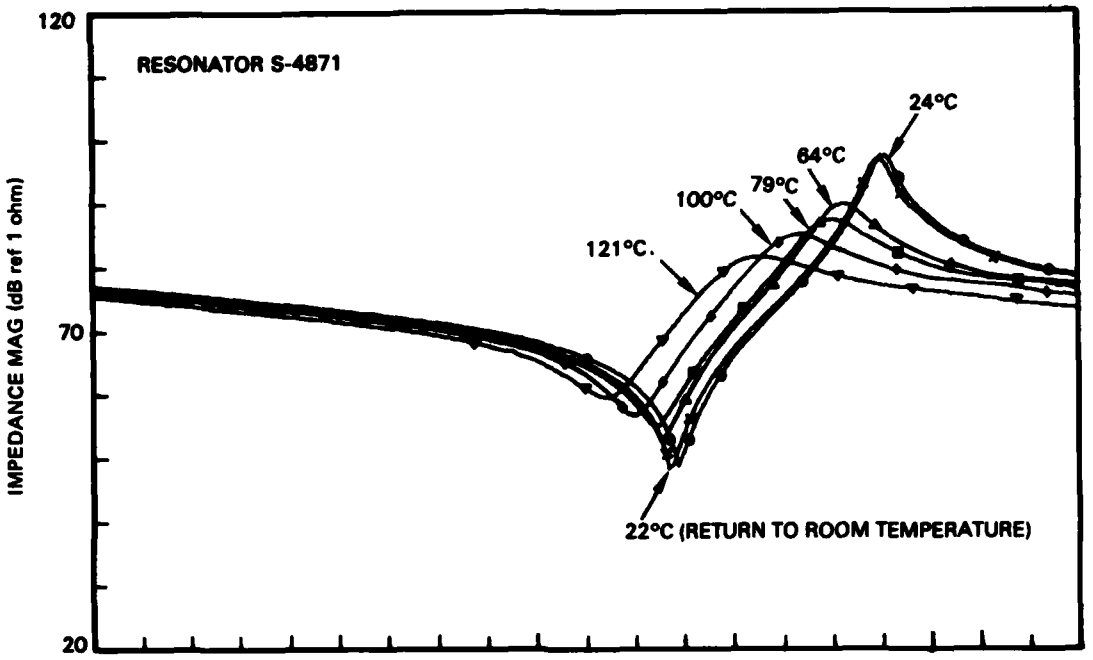

Figure 7a. Oven measurements for a resonator taken from a transducer that was somewhat resistant to current/thermal runaway.

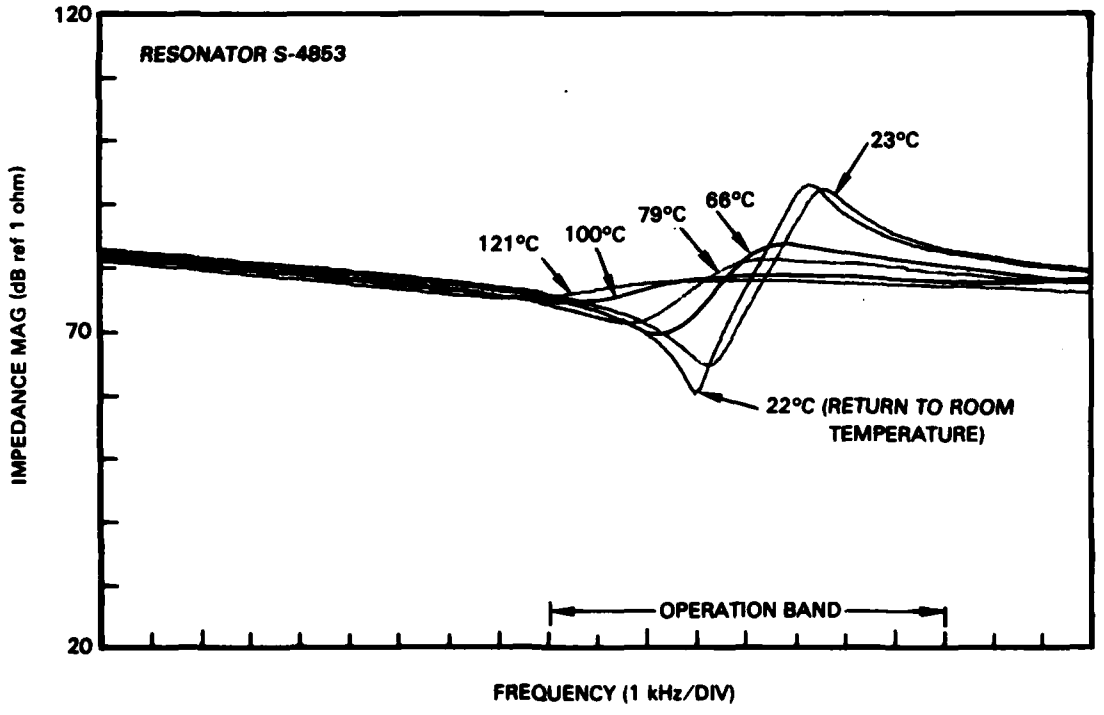

Figure 7b. Oven measurements for a resonator taken from a transducer that was very susceptible to current/thermal runaway.

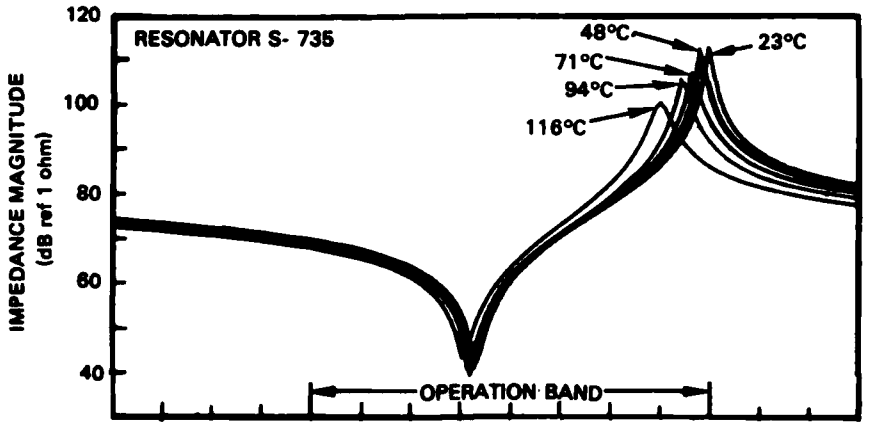

Figure 8. Oven measurements for a resonator that was assembled with a high stress bias (2.8×10^7 Pa).

(4000 psi). The improved performance for such a stressed resonator is shown in Figure 8. It was felt that the higher initial cure stress reduced the amount of cement in the joints.* As a result of these initial tests, it was concluded that the runaway phenomenon was linked to a temperature sensitivity in the cement/electrode** joints of the resonators, with associated self-heating in the joints perhaps compounding the problem.

2.0 OBJECTIVES

The present report documents the continuation and conclusion of a task that began in FY81. The initial phase of the task was described recently in a NOSC interim Technical Report.† The objectives have been to:

1. Understand the role of cement/electrode joints in the temperature sensitivity of ceramic-stack resonators.
2. Understand, in turn, the mechanism by which the resonator temperature sensitivity causes current/thermal runaway.
3. Determine improved resonator designs or assembly techniques to eliminate or limit the degrading effects of temperature.

---

* This conclusion will be reevaluated in this report.

**Both the electrode and the cement appear to play a role in the joint behavior.

†C.L. Goodhart et al, Temperature Effects in Ceramic Resonators Containing Cement Joints (Interim Report), NOSC TR 716, June 1982.

3.0 APPROACH

The approach was threefold. First, further understanding of the resonator temperature sensitivity was sought by experimental examination of resonators that were assembled with various joint configurations and/or assembly methods. Second, the pertinent parameters of cement/electrode joints were experimentally determined as a function of temperature. Third, the joint-parameter data were applied to computer models of a ceramic-stack resonator and a transducer of the type that exhibited the current/thermal runaway behavior. The computer models were exercised in various parameter variations in order to pursue the above objectives.

4.0 RESULTS

4.1 FY81 RESULTS

The interim report* discussed the first portion (FY81) of the investigation into the temperature sensitivity of ceramic-stack resonators and its role in the current/thermal runaway phenomenon. That report is briefly summarized in this section.

Experimental results showed that the temperature sensitivity was dependent on the stress bias** applied to the resonator and on whether or not cement was used in the joints. A higher stress bias resulted in a decreased temperature sensitivity and better overall performance. Cementless resonators were less sensitive to temperature than cemented resonators, although the cementless resonators showed signs of poor coupling between ceramic rings. The temperature sensitivity appeared to be linked mainly to a temperature dependence of the cement/electrode joint properties. However, there was an indication that stress bias relief, resulting from thermal expansion differences in the resonator, contributed somewhat to the temperature sensitivity.

---

*NOSC TR 716.

**Initial and final stress were always the same.

A computer model of a ceramic-stack resonator was used to show that resonators assembled with a high stress bias contained stiffer, less lossy joints. It was suggested that the high initial stress was the improving factor; high initial stress would squeeze more cement out of the joints, making them stiffer and less likely to cause temperature sensitivity. The independent effects of initial stress and final stress were not investigated, ie, the initial stress bias was always the same as the final stress bias. In the present report, the effects of initial and final stress are examined independently from one another, with significant results.

4.2. FY82 RESULTS

4.2.1 Evidence of the Importance of Final Stress Bias

One of the most striking results of the present study was obtained upon investigation of the individual importance of the initial and final stress bias to temperature sensitivity. Experimental in-air measurements were obtained in the fashion demonstrated in Figure 4 for resonators with various amounts of initial and final stress bias.

Figure 9 shows that the temperature sensitivity of an unstressed resonator (Figure 9b) is dramatically increased, compared with a stressed resonator (Figure 9a). The results of Figure 9 are for two resonators that were initially constructed in exactly the same manner, with an initial stress (during cement curing) of about 6.9×10^6 Pa (1000 psi). Resonator S-3948 (Figure 9a) was then given a final stress equal to the initial stress.* Resonator S-4167 (Figure 9b) was completely unstressed by removing the stress rod and nut. The unstressed resonator shows dramatic sensitivity to temperature, compared with the stressed unit. In addition, the unstressed resonator does not return to its initial performance after heating. Specifically, it becomes less stiff (f_m and f_n decreased), provides less coupling (Δf decreased), and is more

* The epoxy flows a little before it actually sets, which can reduce the final stress on the resonator unless it is restressed after the cure.

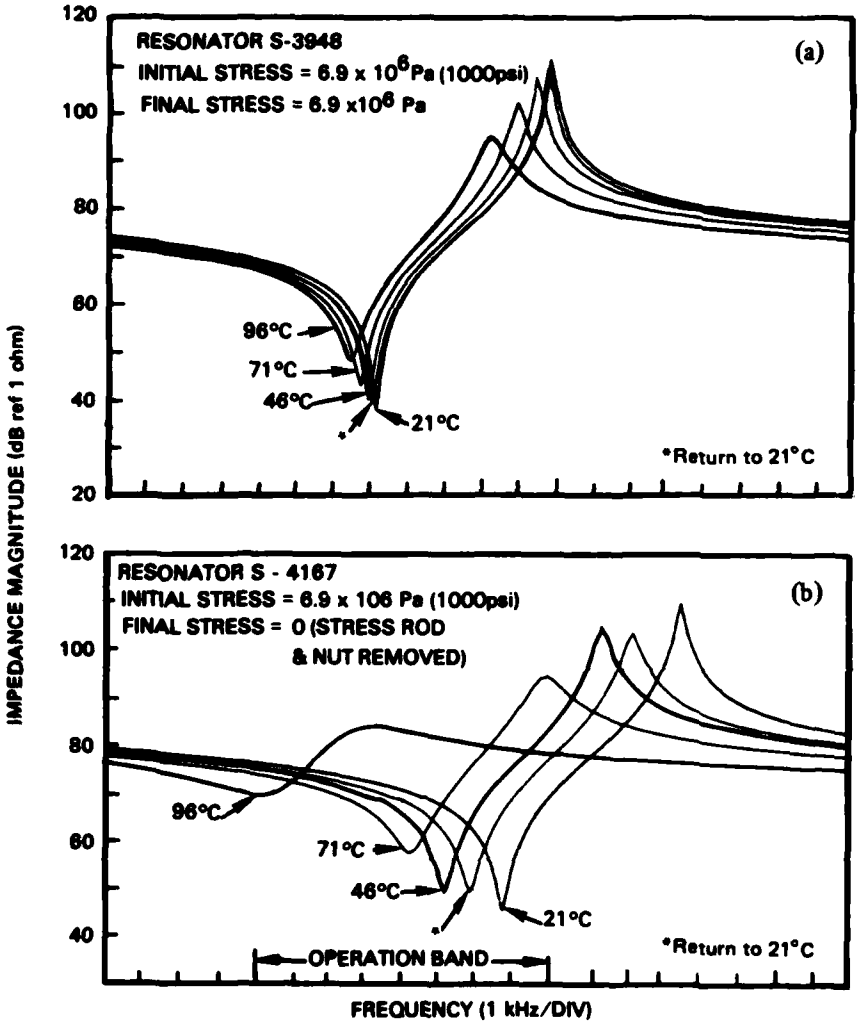

Figure 9. Oven measurements for two resonators; (a) one with a typical final stress bias, and (b) the other with no final stress bias.

lossy (ΔZ decreased). This suggests that the cement bonds in the joints were breaking down, perhaps separating from the ceramic surfaces during heating.

Figure 10 shows results for two resonators that were initially stressed differently but then given final stresses that were equal. NOSC 1 (Figure 1a) was cured* with about 2.8 x 10^7 Pa initial stress** applied and then measured. NOSC 4 (Figure 10b) was cured with an initial stress of about 6.9 x 10^6 Pa then finally stressed to 2.8 x 10^7 Pa before being measured. Notice that the two resonators exhibit very similar temperature behaviors. When the final stress on both resonators was reduced to about 6.9 x 10^6 Pa (Figures 10c and d) they again behaved alike, both performing worse than with the higher final stress. In Figure 11a resonator NOSC 2' is a resonator that was assembled with a high initial stress, like NOSC 1, but given a final stress that was just finger tight. In Figure 11b NOSC 5' is a resonator that was assembled with a low initial stress, like NOSC 4, but given a final stress that was slightly more than finger tight. From these two resonators we see behavior that is somewhat similar to the unstressed resonator in Figure 9b, which is reasonable since these units are just barely stressed. Note also that the slight amount of stress difference between the two resonators in Figure 11 appears to make a difference.

These results indicate, regarding temperature sensitivity, that the final stress on a resonator is more crucial than the initial stress. The temperature-related performance degradation increases as the final stress decreases. Although the degradation is most significant when the resonator is nearly unstressed it is notable that significant degradation occurs when the final stress is reduced from 2.8 x 10^7 Pa to 6.9 x 10^6 Pa (Figures 10a,c and 10b,d). In our cases, where resonators were initially stressed to at least 6.9 x 10^6 Pa, the value of initial stress had no apparent impact on the temperature sensitivity.

---

* All NOSC-built units were cured at 66°C for 2.5 hours and then heat-soaked at 121°C for 2.5 hours before being measured.

**This resonator was not restressed, and thus had a final stress of about 1.5 x 10^7 Pa as determined later by measuring the charge that developed while unstressing the resonator. When later restressed to a full 2.8 x 10^7 Pa the behavior was very similar to that for the 1.5 x 10^7 Pa stress (Figure 10a).

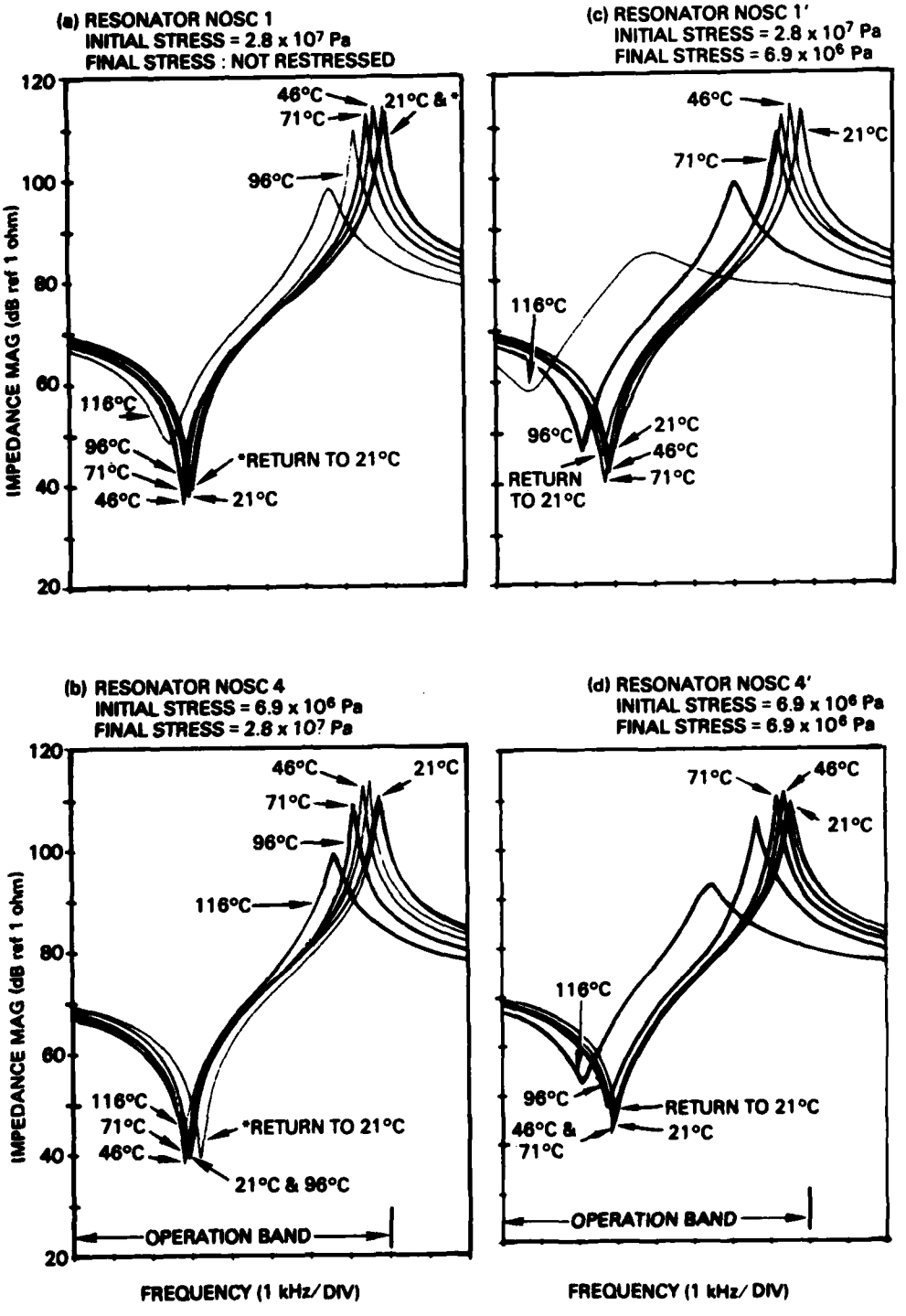

Figure 10. Oven measurements for two resonators assembled differently but given the same final stress of (a) 2.8×10^7 Pa and then (b) 6.9×10^6 Pa.

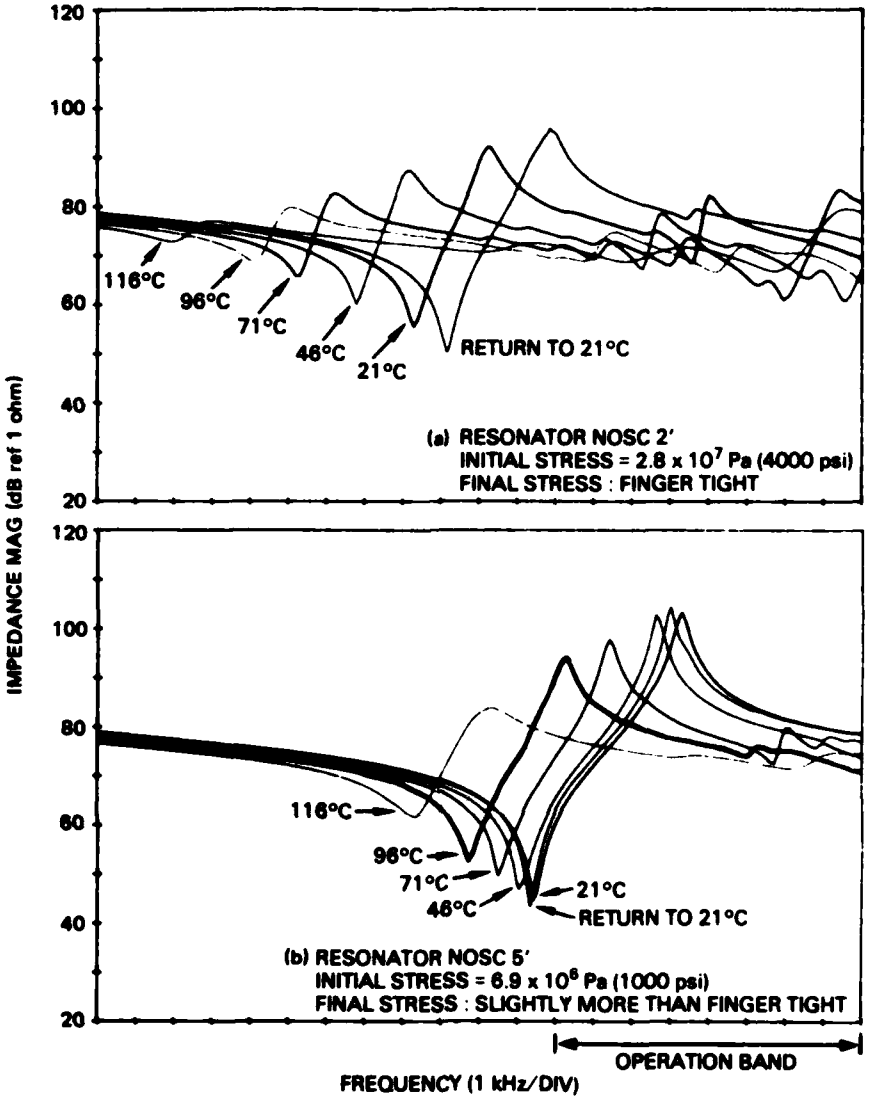

Figure 11. Oven measurments for two resonators assembled differently but each given minimal final stress.

The behavior of an unstressed or nearly unstressed resonator (Figures 9b, 11a and b) is similar to the behavior of the "bad" resonators observed in Figures 6 and 7b. In the first-article transducers such "bad" resonators were probably present for two reasons. First, stress was applied and "measured" with a torque wrench. This could lead to erroneously low stresses due to the presence of burrs, epoxy, or other foreign materials causing seizure of the threads. A better stress method, which is presently used, is to measure the

charge generated by the ceramic during the stressing procedure. Second, some of the resonators had been "fine tuned" in regard to their frequency response by adjusting the final stress bias. "Bad" resonators, such as seen above, can cause the behavior observed in the current/thermal runaway phenomenon, as will be demonstrated later in this report.

4.2.2 Stress-Relief Due to Thermal Expansion

The in-air oven measurements have shown that resonators, other than those that are nearly or completely unstressed, exhibit reasonable stability at low temperatures, with degradation commencing only after some high temperature is reached. This suggests the obvious concern that stress relief may occur due to thermal expansion differences between the stress rod and body portion of the resonator. From Figure 12 the original stretch in the stress rod is given, in metres, by

$$\Delta L_{sr} = \frac{A_c L_{sr} P_c}{A_{sr} E_{sr}} = 1.79 \times 10^{-12} P_c \qquad (1)$$

where E_{sr}, the modulus of the rod, is 2.00×10^{11} Pa; L_{sr}, the rod length, is 4.32×10^{-2} m; A_c, the ceramic area, is 1.69×10^{-4} m^2; A_{sr}, the rod area, is 2.03×10^{-5} m^2; and P_c, the stress bias, is expressed in pascals. This corresponds to a stretch of about 12.4 μm ($.49 \times 10^{-3}$ inches) for a stress bias of 6.90×10^6 Pa (1000 psi), which was the final stress bias called for in the first-article resonators. Thermal expansion in the resonator will relieve the stress rod if the body of the resonator expands less than the stress rod. The excess expansion of the stress rod over the expansion of the resonator body is given, in metres, by

$$\Delta L = [a_{sr} L_{sr} - (a_c L_c + a_a L_a + a_{sw} L_{sw})] \Delta T \qquad (2)$$

where the L's are lengths, a's are thermal expansion coefficients, ΔT is the temperature change in °C, and subscripts designate resonator sections. Using "book" values and the ceramic manufacturer's data for the required expansion coefficients (Table 1), Equation (2) indicates a reduction in the original

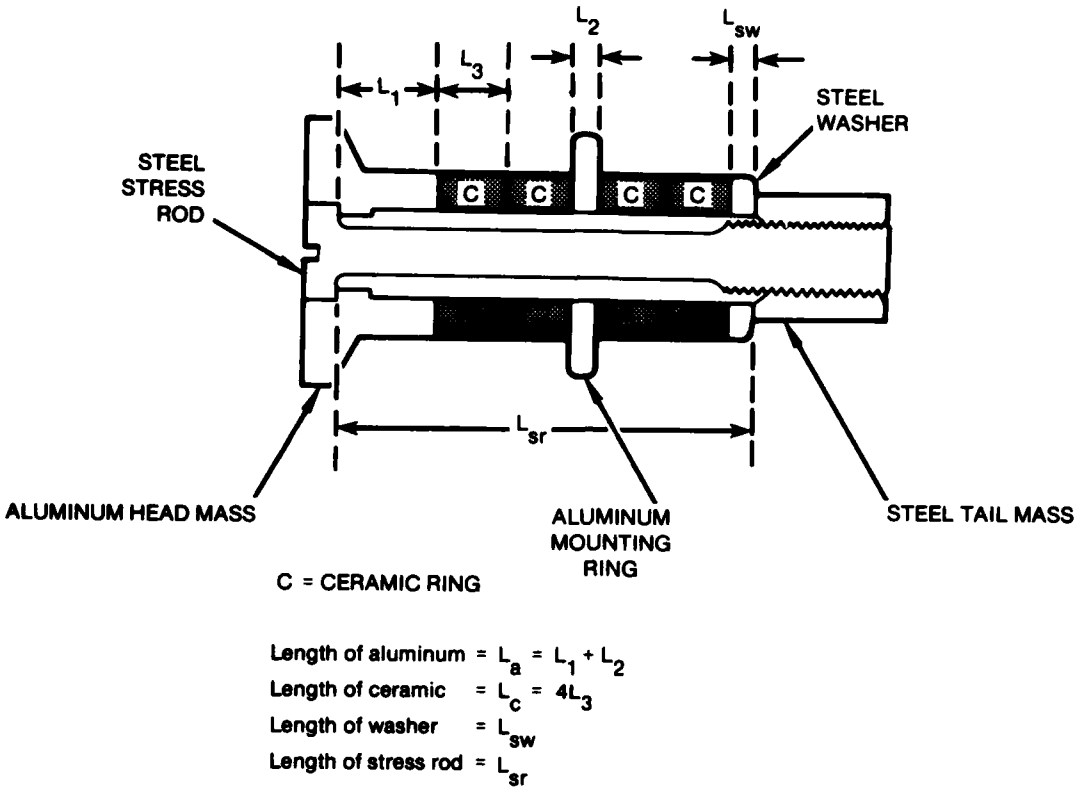

Figure 12. Resonator information for analysis of thermal expansion induced stress relief.

stretch of the stress rod of 1.1×10^{-7} m/°C (2.4×10^{-6} in/°F). The corresponding stress relief, in Pa, is given by

$$\Delta P = E_{sr} A_{sr} \Delta L/(L_{sr} A_c) = 6.2 \times 10^4 \Delta T \qquad (3)$$

Resonator Section	Length (cm)	Thermal Expansion Coefficient (cm/°C cm
Steel Stress Rod	4.32	1.1×10^{-5}
Ceramic	2.84	1.7×10^{-6}
Aluminum	1.19	2.4×10^{-5}
Steel Washer	.28	1.1×10^{-5}

Table 1. Lengths and thermal expansion coefficients for the resonator sections that are pertinent to stress relief.

Table 2 lists the stress relief that would occur for various temperature changes.

ΔT(°C)	ΔP(10^6Pa)	ΔT(°F)	ΔP(psi)
28	1.6	50	230
56	3.2	100	460
111	6.3	200	920

Table 2. Calculated stress relief resulting from thermal expansion.

During CUALT, the internal temperature in one of the runaway transducers rose from about 16°C to nearly 116°C. This would relieve nearly the entire stress on the first-article resonators (6.9×10^6 Pa). In fact, in some resonators the stress would have been relieved at much lower temperatures because of the erroneously low stress biases that we suspect existed.

Differences between the actual expansion coefficients and the "book" values used above could significantly change the results of the analysis. For example, although not demonstrated here, a 4% error of each thermal expansion coefficient in a proper direction would result in no stress relief with heating ($\Delta L=0$). Nonetheless, the analysis shows that significant stress relief could have occurred due to thermal expansion.

4.2.3 Electrode Importance

One final issue is important here: the electrode plays some part in the joint temperature and stress sensitivity. Figure 13 shows results for a resonator containing solid soft brass electrodes but no cement. In Figure 13a the resonator was stressed to 4.8×10^6 Pa (700 psi) and in Figure 13b to 2.8×10^7 Pa (4000 psi). At the lower stress (Figure 13a), the resonator is very sensitive to temperature in a fashion somewhat similar to, although more exaggerated than, very low-stressed resonators that contain nickel expanded-metal electrodes and cement (Figures 9b and 11a and b). At the higher stress (Figure 13b) the resonator again behaves similarly to resonators with expanded-metal electrodes and cement (Figures 10a and b), except at 116°C,

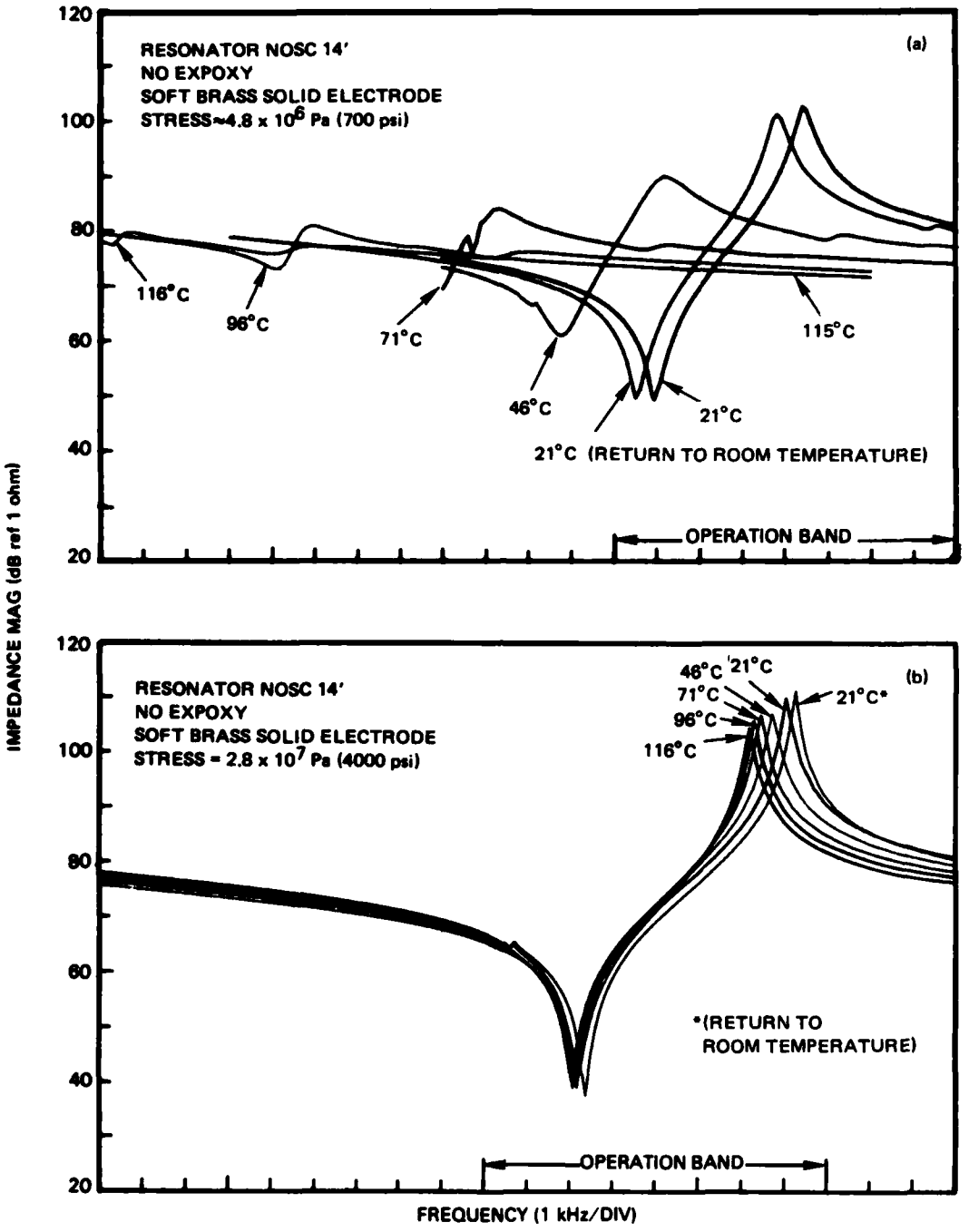

Figure 13. Oven measurements for a cementless resonator with (a) low and (b) high stress bias.

where it does not behave as badly. Apparently a cementless resonator possesses temperature sensitivity and final stress sensitivity that are in some ways similar to the sensitivities in a cemented resonator. This means that something, in addition to the cement, contributes to the temperature and stress sensitivity. Other possibilities are:

1. Temperature dependence of ceramic parameters
2. Stress dependence of ceramic parameters
3. Temperature dependence of electrode parameters
4. Stress dependence of electrode parameters

Item 1, the temperature dependence of ceramic parameters, is ruled out on the basis of the results of Figure 14. This figure shows impedance magnitude vs frequency curves for a modeled resonator at three temperatures. The ceramic parameters that were used in the model were measured, for free rings at the three temperatures (see Appendix). The effect of temperature predicted by the model is the opposite from that which is experimentally observed. Increasing the temperature alters the ceramic parameters and causes the impedance vs frequency response of the resonator to shift up in frequency rather than down. Item 2, the stress dependence of ceramic parameters, cannot be ruled out as a contributor, because we do not know the parameter vs stress relationships. As a matter of fact it seems likely that it plays more of a role at high stress biases where cement joint parameters are less prominent. However, the drastic behaviors observed for unstressed or nearly unstressed resonators are obviously not a result of unstressing the ceramic. Item 3, temperature dependence of electrode parameters, is discounted simply because a metal, even a soft metal, would not be expected to have much temperature sensitivity over the temperature range of concern. Item 4, stress dependence of electrode parameters, is a likely contributor to temperature and stress sensitivity. More specifically, though, it is probably the manner in which the expanded-metal electrode makes contact with the ceramic under different stresses that is important. Thus, the cement and the electrode or cement/electrode joints are the factors in the temperature sensitivity problem.

4.2.4 Cement/Electrode Joint Parameter Measurements

The cement/electrode joint properties that are of concern are the joint modulus (or, equivalently, the joint stiffness) and the associated loss factor. In order to determine the cement joint properties as a function of temperature, we matched the results of a plane-wave computer model of a dumbbell resonator to experimental measurements of real dumbbells (Figure 15). At the outset of this discussion of joint parameter determinations, it is important to realize that the method used here ascribes the temperature-related behavior of a dumbbell resonator to changes in the parameters of composite cement/electrode joints. Each joint is modeled as a plane wave section of homogeneous material. Thus, although the results do not provide the temperature behavior of the cement or the electrode individually, they do yield composite joint parameters that simulate the real resonator behavior no matter what the details of the temperature sensitivity mechanism.

Three dumbbells were constructed, each containing two ceramic rings for excitation and three cement/electrode joints (Figure 15). The dumbbells were designed to bring the second longitudinal resonance into the frequency band of interest. The construction of each dumbbell differed in the type of electrode used and the amount of stress applied during the epoxy cure (Table 3). The dumbbells were not restressed after the cement cure, therefore, because of flow, the final stresses are assumed to be somewhat less than the initial stresses. Hysol EA8 epoxy (previously Shell EPON VIII) was the cement used in each dumbbell. It was cured at 66°C for 2.5 hours.

Dumbbell	Electrode	Stress (10^6 Pa)
1	expanded-metal	6.9
2	expanded-metal	28.0
3	solid	6.9

Table 3. Construction of three dumbbell resonators.

The measurements of the resonant and antiresonant frequencies, and their associated impedance magnitudes were made at five temperatures for the three

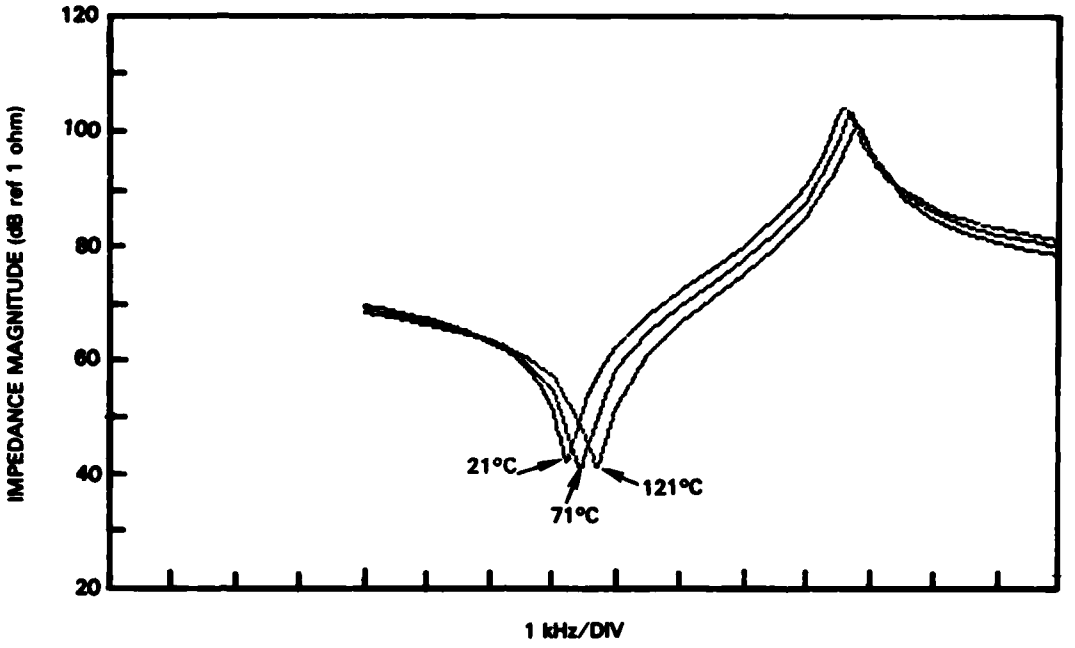

Figure 14. Modeled resonator behavior resulting from temperature effects on ceramic alone.

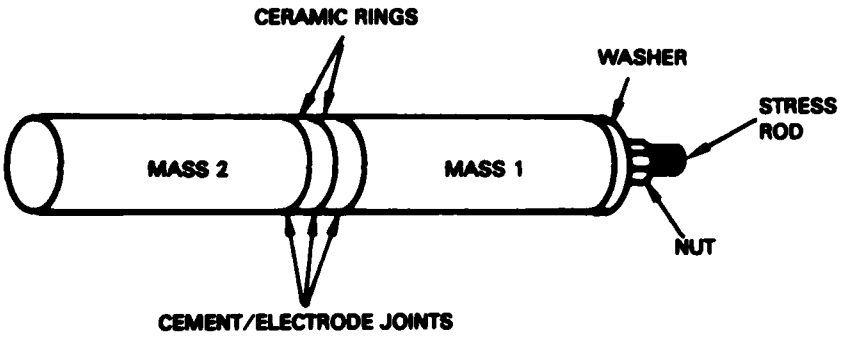

Figure 15. Dumbbell for cement/electrode properties determinations.

dumbbells, using the method and equipment described in the Appendix. Figure 16 shows results for the resonant and antiresonant points for each of the dumbbells. The temperature behavior of the dumbbells is, in general, the same as that of the resonators, ie, f_m, f_n, Δf, and ΔZ all decrease with rising temperature. All three dumbbells exhibit similar behavior at first, but dumbbell three shows dramatic degradation between 96°C and 121°C. Stress relief calculations indicate that, between 21°C and 121°C, the dumbbells relieve about 3.5×10^6 Pa of the stress bias, which is about half of the low initial stress value. Considering that the dumbbells were not restressed after curing, perhaps significant stress relief is present in dumbbell one above 96°C, causing the dramatic shift. Dumbbell three did not exhibit similar behavior, although it was stressed the same as dumbbell one. This may be a result of the solid electrode in dumbbell three as opposed to the expanded-metal electrode in dumbbell one. In any case, the experimental temperature sensitivity of dumbbell one is representative of a "bad" resonator (Figures 6 and 7b), particularly in the total frequency shifts of f_m and f_n between 21°C and 121°C.

The dumbbells were modeled using a plane-wave computer model. The moduli for the stress rod and end-masses were obtained by careful measurements of the density and sound velocity (via the resonance method) in the materials. The ceramic parameters were taken from the MAST (see Appendix) free-ring measurements for the specific rings used in each dumbbell. The effect of stress on the ceramic rings was not available and thus was not included. For the thin composite cement/electrode joints the essential parameter is the effective complex stiffness, which is given by

$$K = EA/L \tag{4}$$

where E is the complex joint modulus, A is the joint area, and L is the joint length. The joint stiffness loss factor is given by

$$KM = K_i/K_r \tag{5}$$

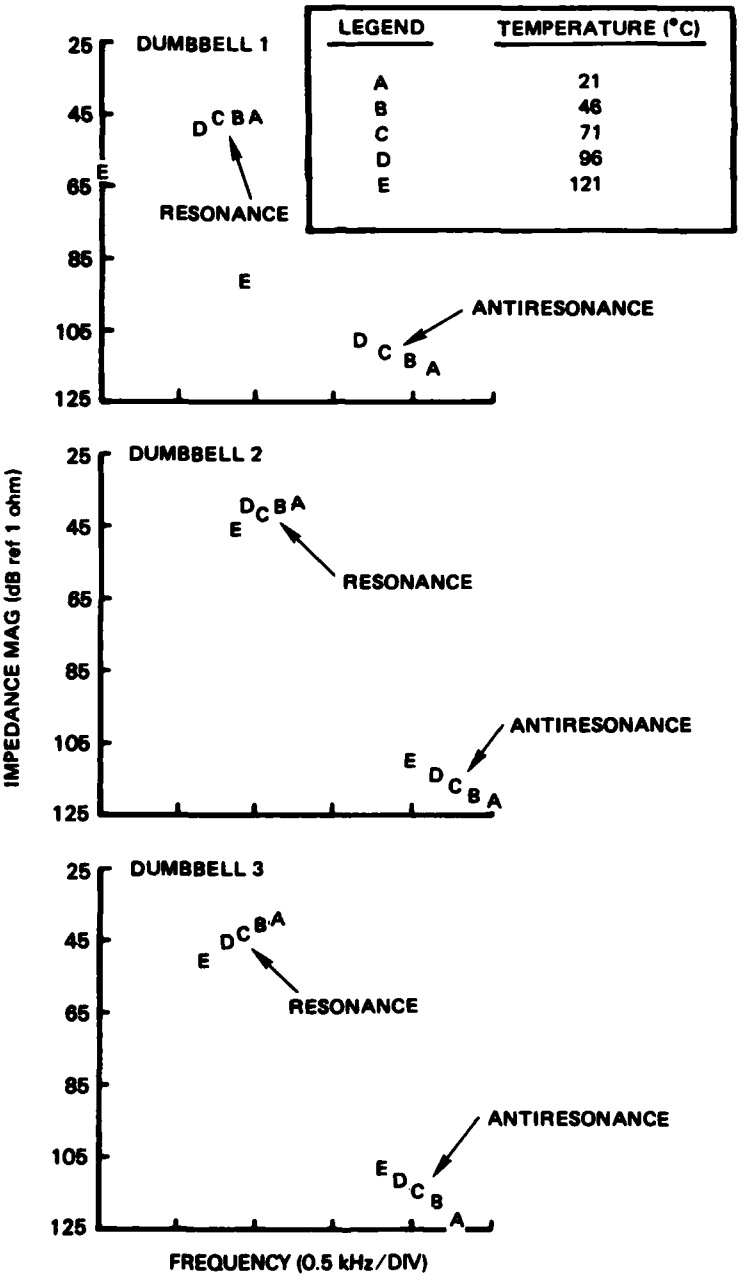

Figure 16. Experimental results for a temperature dependencies of the resonances and antiresonances of three dumbbell resonators.

where K_i and K_r are the real and imaginary parts, respectively, of the complex joint stiffness.

The complex joint modulus was found for each dumbbell by adjusting the joint modulus in the model in order to match the modeled resonant frequency and associated impedance magnitude to the experimental measurements. Figure 17a gives the resulting joint stiffnesses for the two dumbbells that contain expanded-metal electrodes. The stiffness for the high-stress dumbbell-(dumbbell two) drops 76% between 21°C and 121°C, and the corresponding drop for the low-stress dumbbell (dumbbell one) is 84%. Such stiffness changes will later be shown to have a significant impact on the behavior of a computer model of the transducer that exhibited current/thermal runaway behavior. The joints for the low-stress dumbbell are about half as stiff as those for the high-stress dumbbell except at 121°C, where they are only one-third as stiff due to a sharp drop in the stiffness of the low-stress joints. The calculated stiffness of all cement residing in the holes of the expanded-metal electrode is approximately 7.7×10^9 N/m at 21°C, and the calculated stiffness of just the exmet electrode is approximately 1.8×10^{11} N/m. Thus, the deduced joint stiffnesses seem reasonable. But again, it is pointed out that the electrode and cement apparently do not independently behave in a plane-wave fashion; if they did, the electrode would dominate due to its high stiffness. The temperature behaviors of the joint loss factors are shown in Figure 17b, as deduced from the dumbbell measurements and computer model. As expected, the low-stress dumbbell exhibits the larger loss factor. The result of the initially decreasing loss factor as the temperature rises, as seen in both dumbbells, is somewhat unexpected and is not understood.

Figure 18 shows the in-air impedance magnitude vs frequency response for a resonator model that employs the joint parameters that were determined from the low-stress dumbbell. The modeled resonator predicts, at room temperature, an f_m and f_n that are, respectively, approximately 1.9 kHz and 2.9 kHz above those observed in the "bad" resonator of Figure 6. One reason for this is an extra 8% stiffness in the joints of the resonator model due to an oversight in the model inputs. Concerning the impedances: because $1/\Delta Z$ is a measure of

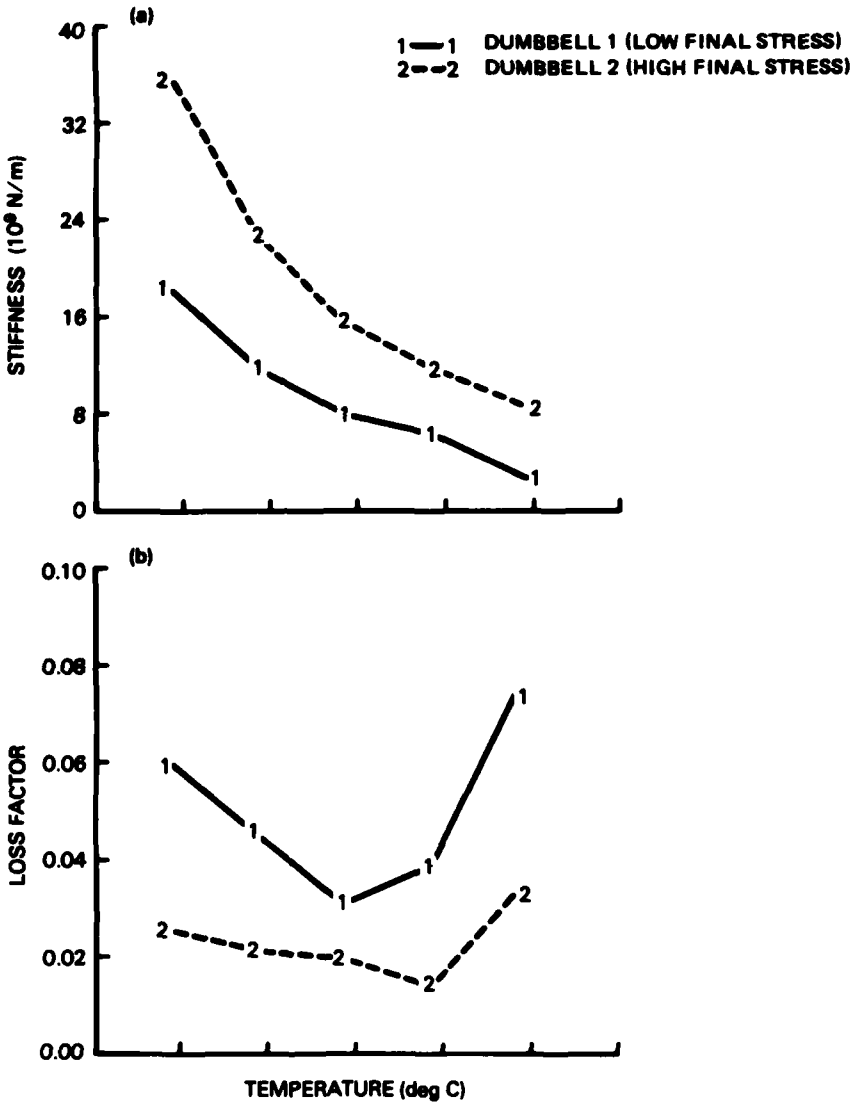

Figure 17. Experimentally determined complex joint stiffness for the cement/electrode joints of two dumbbells.

the resonator losses, the joints in the "bad" resonator appear to be significantly more lossy than those determined from dumbbell one. In the investigation of temperature sensitivity, the changes with temperature are the important features. The reduction in ΔZ with increasing temperature is difficult to compare because the initial ΔZ is much less for the actual resonator than for the model. The total frequency shifts of f_m and f_n with temperature are similar, although somewhat less in the model than in the actual resonator (this is especially true in light of the fact that ceramic effects, which cause some shift upward in frequency (Figure 14), have not been included in the model). The similarity of shifts in f_m and f_n between the model (Figure 18) and the actual resonator (Figure 6) indicates that the joint parameters for the low-stress dumbbell are representative of a "bad" resonator mainly in the temperature-related stiffness behavior, between 21°C and 121°C.

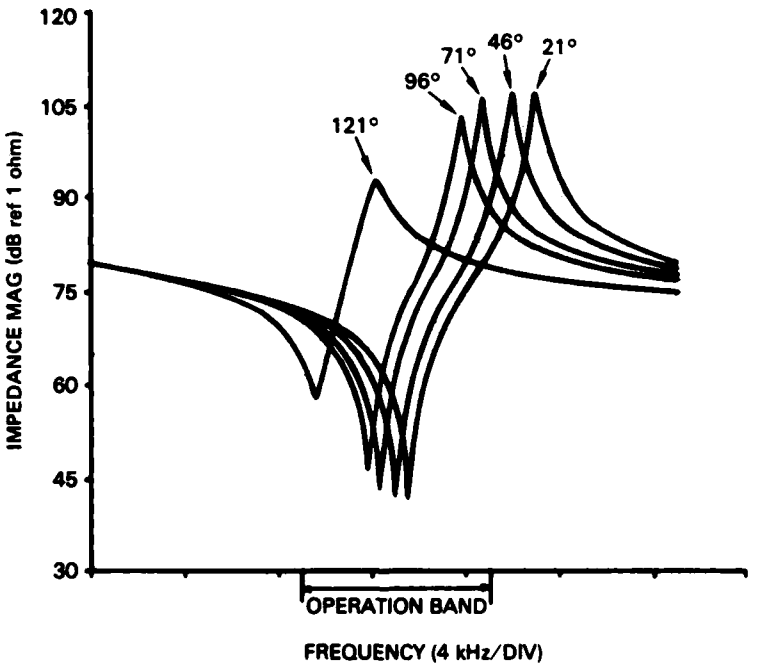

Figure 18. Temperature dependence of a computer modeled resonator, using the cement/electrode joint parameters from the low-stress dumbbell.

There are some important cautions to be noted. The method of determining joint parameters from ceramic-driven dumbbells is a sensitive procedure because the presence of the joints may cause only small effects, especially at

low temperatures. For example, according to modeling results, in an expanded-metal electroded dumbbell that contains three joints, the resonance is only about 2% less than the resonance for the same resonator with no cement joints. This requires accurate measurements of the ceramic parameters, the properties of the other dumbbell components (lengths, areas, and moduli), and the experimental measurements of the dumbbells.

One check on the joint parameter determinations is to compare the frequency and impedance magnitude at antiresonance for the actual dumbbell and the model. (The frequency and impedance magnitude at resonance agree because they were matched between model and experiment in order to find the joint parameters.) Table 4 makes this comparison for the two dumbbells with expanded-metal electrodes. A brief sensitivity study showed that an error of 0.4% in the antiresonant frequency, f_n, could yield a 31% error in the determination of both the stiffness and loss factor at 21°C and 8% at 121°C. A factor of 2 (6 dB) error in the maximum impedance, Z_n, could cause a factor of 2 error in the joint loss factor determination at both 21°C and 121°C. From this perspective, Table 4 suggests that the worst error in the joint stiffness determination may be somewhere around 16% for the two dumbbells. The error in loss factor, on the other hand, may be very large at times, especially for the high-stress dumbbell at 96°C.

Finally, the third dumbell, which contained solid nickel electrodes and has not yet been discussed, yielded an experimental resonance that was 1.3% higher than the model could yield even with infinitely stiff joints. This problem is not yet solved.

Dumbbell	Parameter	Temperature (°C)				
		21	46	71	96	121
1	f_n	.0	.1	.3	.4	.9
1	Z_n	2.0	1.9	-.2	.3	-2.8
2	f_n	-.2	-.2	-.3	-.3	-.2
2	Z_n	4.5	4.0	3.7	4.6	2.5

Table 4. Difference in f_n(%) and Z_n(dB) between the experimental and model results.

The results of the joint parameter determinations are not as satisfactory as had been hoped, particularly regarding the loss factor. One probable reason for this is the unknown effects of stress on the ceramic rings, since the ceramic parameters were determined on unstressed rings but the joint parameters were determined from dumbbells that were stressed. Using a dumbbell without ceramic rings would eliminate this problem. Such a dumbbell could be excited with mechanical impulses at the end of the dumbbell. Unfortunately, at the beginning of the present effort, no environmental chamber of sufficient size was available to house both the dumbbell and an impulse device. In summary, the stiffness determinations that we have obtained seem reasonable, considering the expected stiffnesses for only cement or electrodes in the joints, and considering the results of Table 4. The findings are sufficient to provide significant insight into the fundamental principles involved in the current runaway phenomenon. These principles are discussed next.

4.2.5 Transducer Modeling Results

We have seen that ceramic-stack resonators that contain cement/electrode joints demonstrate a sensitivity to increasing temperature that becomes especially pronounced under low final stress biases. The conclusive details or mechanisms involved in the temperature sensitivity have not been ascertained. Nonetheless, we have reproduced the behavior, in part, in a resonator model by attributing the behavior to the temperature dependence of composite cement/electrode joint parameters. The temperature sensitivity provides significant insight into the transducer current/thermal runaway phenomenon when examined from a modeling approach as is now discussed.

A computer model of the transducer (Figure 2) was developed consisting of five identical pralleled resonators in series with a tuning inductor and transformer. In addition, radiation loading was included in order to account for immersion of the transducer in water. The resonator joint parameters were taken to be those that were obtained from the low-stress dumbbell. The ceramic parameters were taken from "book" values and were held constant over all the temperatures; the effects of temperature on the ceramic (Figure 14) are overshadowed by the effects on the joints. Figure 19 shows the resulting transducer input current magnitude and phase as a function of frequency for

five temperatures. The cement/electrode joint parameters are supplied at the top of the figure. Because the drive is a constant-voltage source, the current magnitude can be viewed as impedance except for a constant. Two points should be made here prior to examining these results. First, f_m and f_n were higher in the model than in the actual transducer. Second, the current at f_n was less in the model than in the actual transducer (by between 6 to 9 dB). Many items not included in the model could affect these values, such as the 8% joint stiffness oversight previously mentioned, the nodal mounting of the resonators, the ambient oil, the rubber window, etc. In any event, of main interest was the relative changes with temperature and not the absolute levels. Therefore, the above discrepancies are not relevant. In the actual transducer the operation band is centered about f_n, thus the operation band has been positioned accordingly in the figure.

The main features seen in the figure are a resonance and antiresonance, essentially related to those of the resonators, and also a higher frequency resonance that turns out to be a series resonance between the tuning inductor and the capacitive-like resonators. As was true for the individual resonators, the most prominent effect of rising temperature is the downward shift of the current response in frequency. Because the operation band is centered about f_n, this behavior brings higher current, or lower impedance, regions into the operation band. If this shift is sufficient to bring the series resonance near or into the operation band, the current rise will become extremely dramatic. At f_o, in Figure 19, the current behavior is similar to that actually observed in the current/thermal runaway phenomenon (Figure 3), both in magnitude and phase. Specifically, as the temperature rises the current magnitude initially drops, then rises dramatically; and in addition, the current phase shows that the admittance changes monotonically from inductive to capacitive values. Actually, current/thermal runaway occurred at the lowest frequency in the operation band. Such behavior is not quite reproduced at that point in the modeling results in Figure 19. However, because of some of the uncertainties mentioned earlier, our modeling is somewhat qualitative, thus the lack of one-to-one frequency agreement is not of great concern. Note that the joint loss factor does not change greatly in the temperature range here. Thus, the current behavior in Figure 19 is essentially a result of a

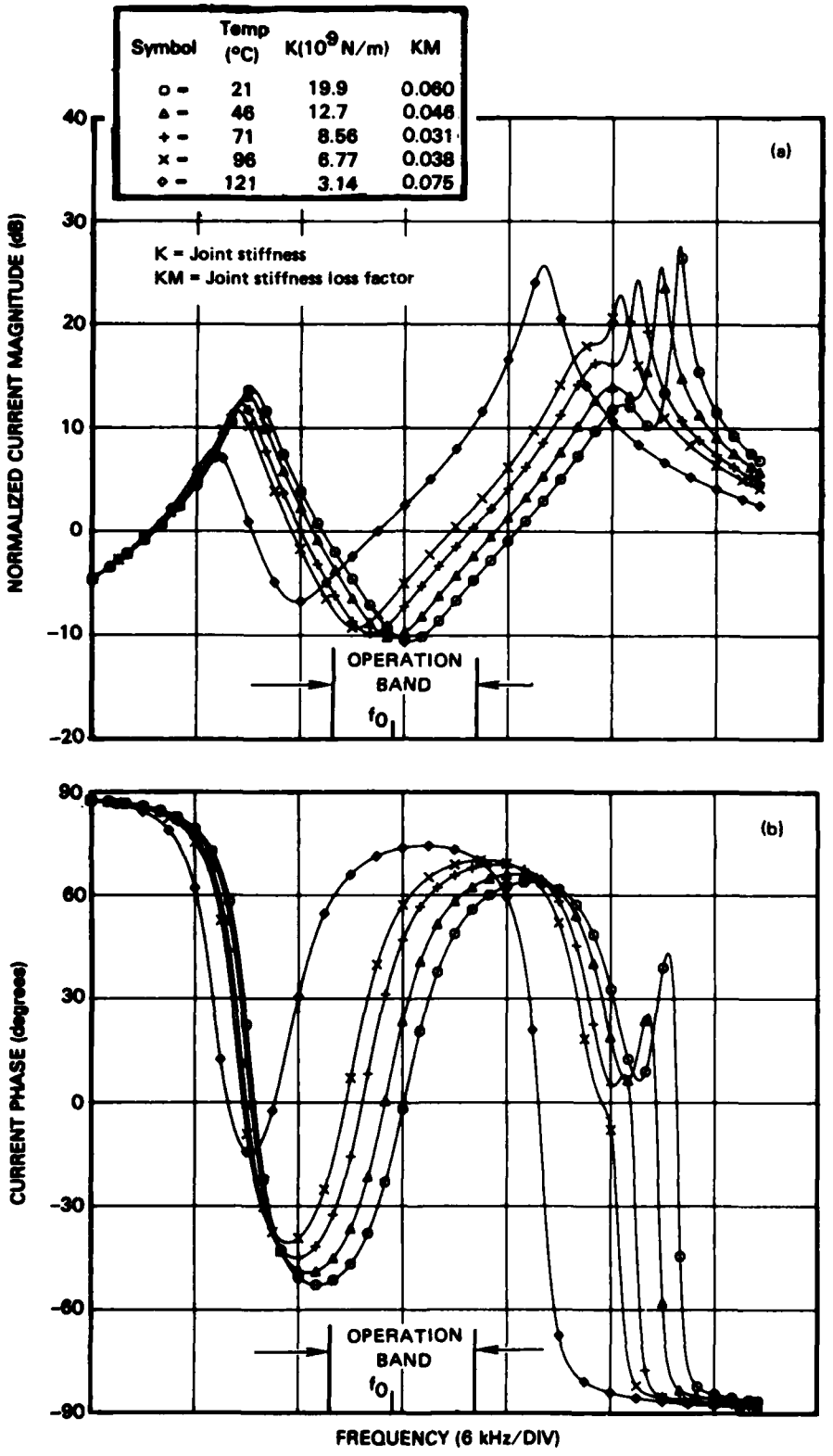

Figure 19. Modeled transducer input current using the cement/electrode joint parameters from the low-stress dumbbell.

joint stiffness that decreases as the temperature rises. (This will be further illustrated shortly.)

Although the current runaway behavior tracks with a joint stiffness that decreases as the temperature rises, the more fundamental problem is to explain the continual temperature rise (thermal runaway aspect). This issue is addressed in part by the results shown in Figure 20a, which indicates the power dissipated in the transducer model at various temperatures. Again examining at f_o, the heating initially remains fairly constant as the temperature rises but finally increases significantly. Figure 20b shows that the transducer becomes increasingly inefficient as the temperature rises. Because the joint loss factor does not change greatly here, these results suggest that thermal runaway may occur due, chiefly, to temperature effects on the joint stiffness and not on the joint loss factor. However, a definitive statement cannot be made because of the uncertainty in the temperature behavior of the joint loss factor.

It is interesting to compare the predicted transducer performance for independent variations of the joint stiffness and the joint loss factor. The joint stiffness was varied between 2.01×10^{10} Pa and 2.23×10^{9} Pa (Figures 21 and 22) and the joint loss factor was varied between 0 and 0.1 (Figures 23 and 24). Figure 21a shows that as the joint stiffness decreases, the current amplitude greatly increases in the operation band. Figure 23a illustrates that loss factor changes do not have a similar effect. The current phase behavior shows that the admittance becomes more capacitive as the joint stiffness decreases (Figure 21b), but changes very little with the loss factor variation (Figure 23b). These results further indicate that it is the joint stiffness and not the loss factor that is directly related to the current behavior that was observed during the current/thermal runaway phenomenon. That is not to say that the loss factor cannot indirectly contribute to the current behavior by being a factor in the thermal aspect of the runaway phenomenon. In fact, both a decreasing joint stiffness and an increasing joint loss factor can give rise to increased heating in the resonator (Figures 22a and 24a), due to an increasing inefficiency (Figures 22b and 24b).

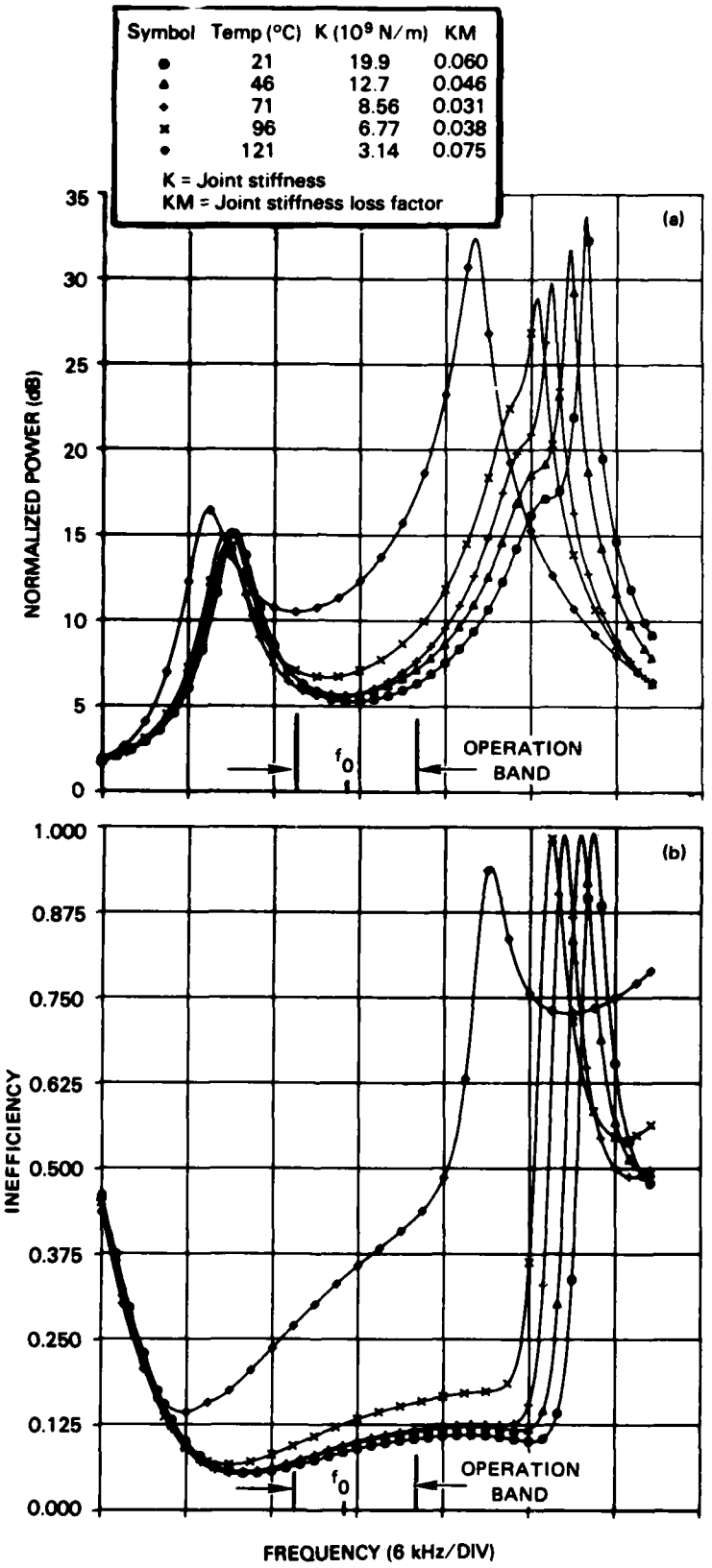

Figure 20. Modeled power dissipation and transducer inefficiency using the cement/electrode joint parameters from the low-stress dumbbell.

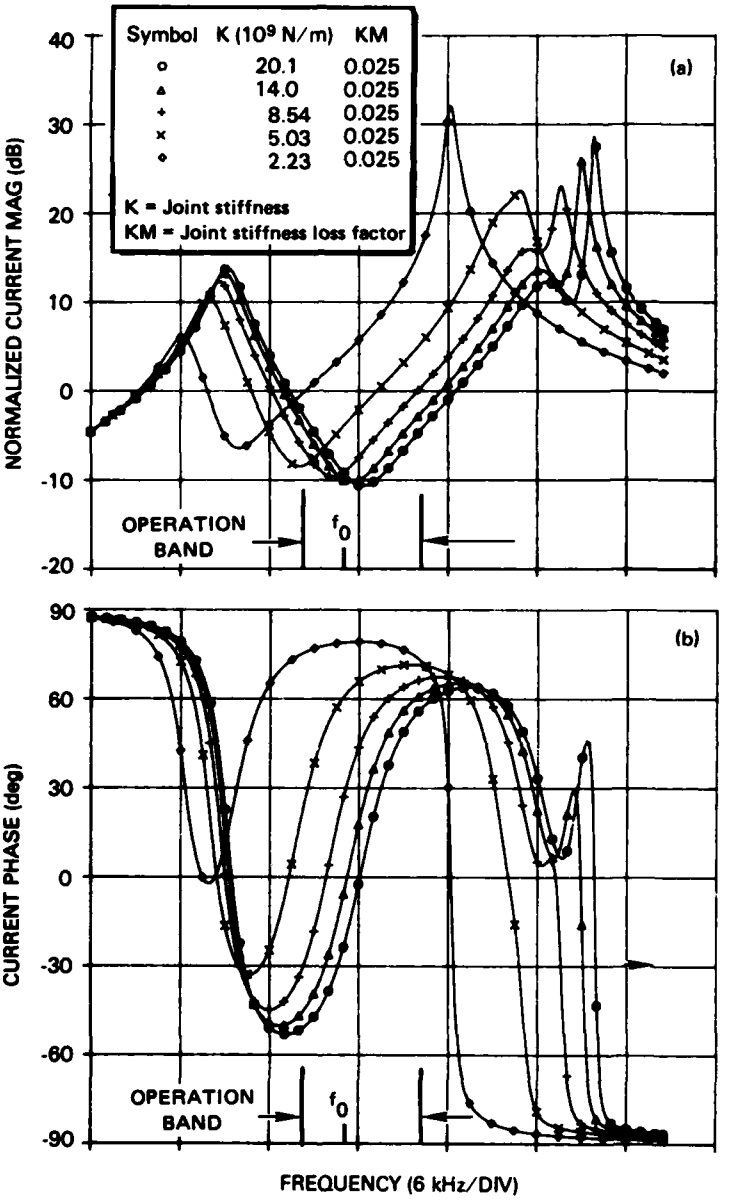

Figure 21. Modeled transducer input current for a variation of joint stiffness in the ceramic-stack resonators.

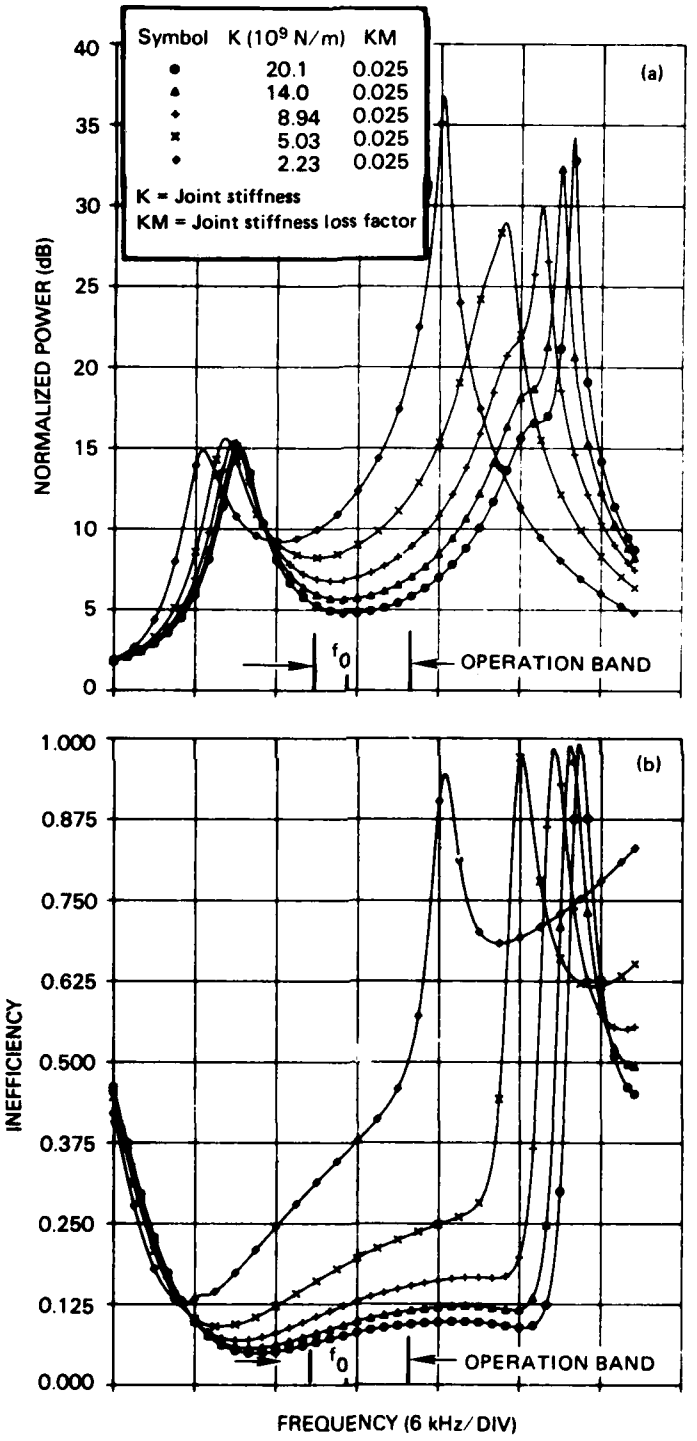

Figure 22. Modeled power dissipation and transducer inefficiency for a variation of joint stiffness in the ceramic-stack resonators.

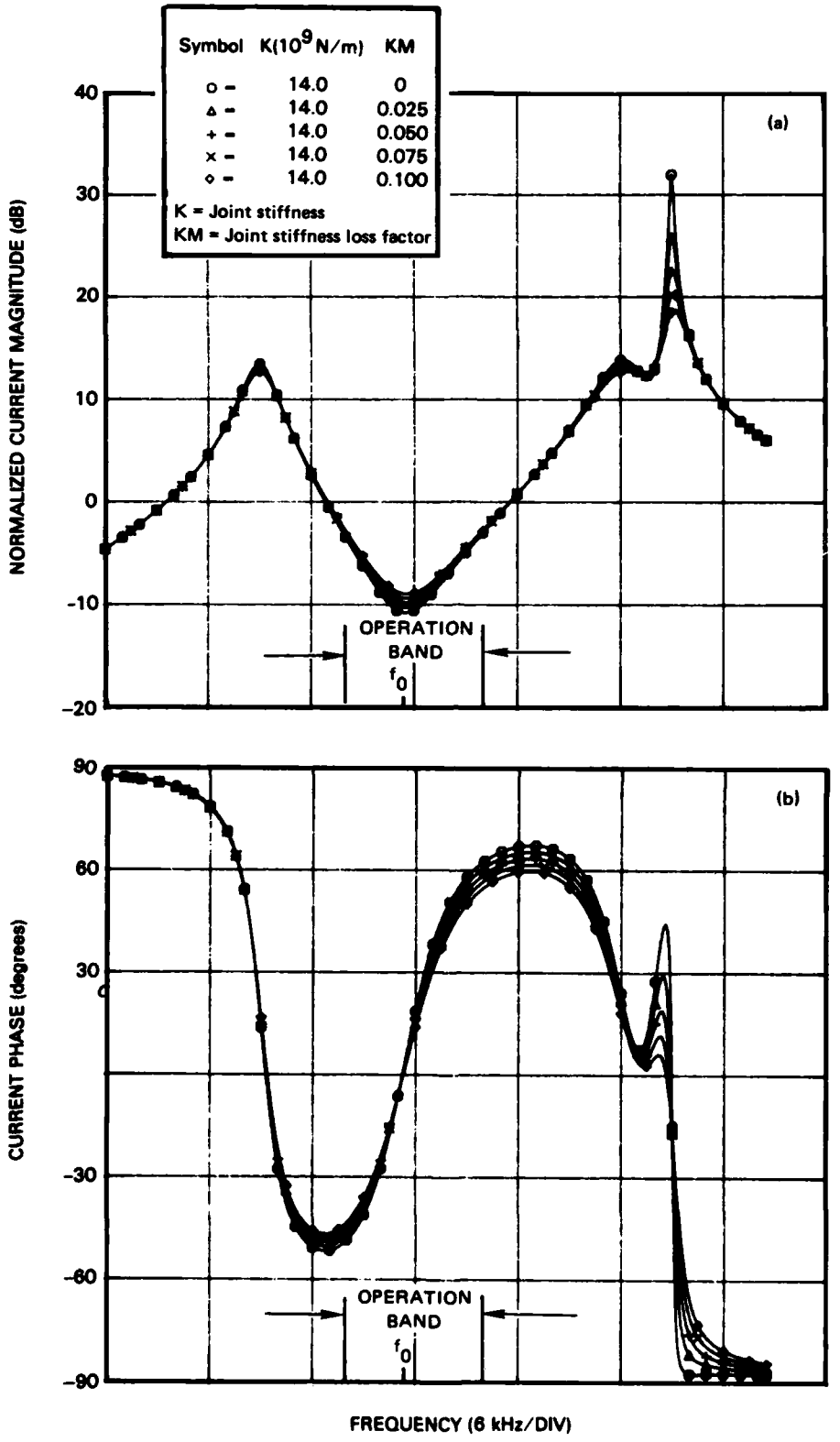

Figure 23. Modeled transducer input current for a variation of joint loss factor in the ceramic-stack resonators.

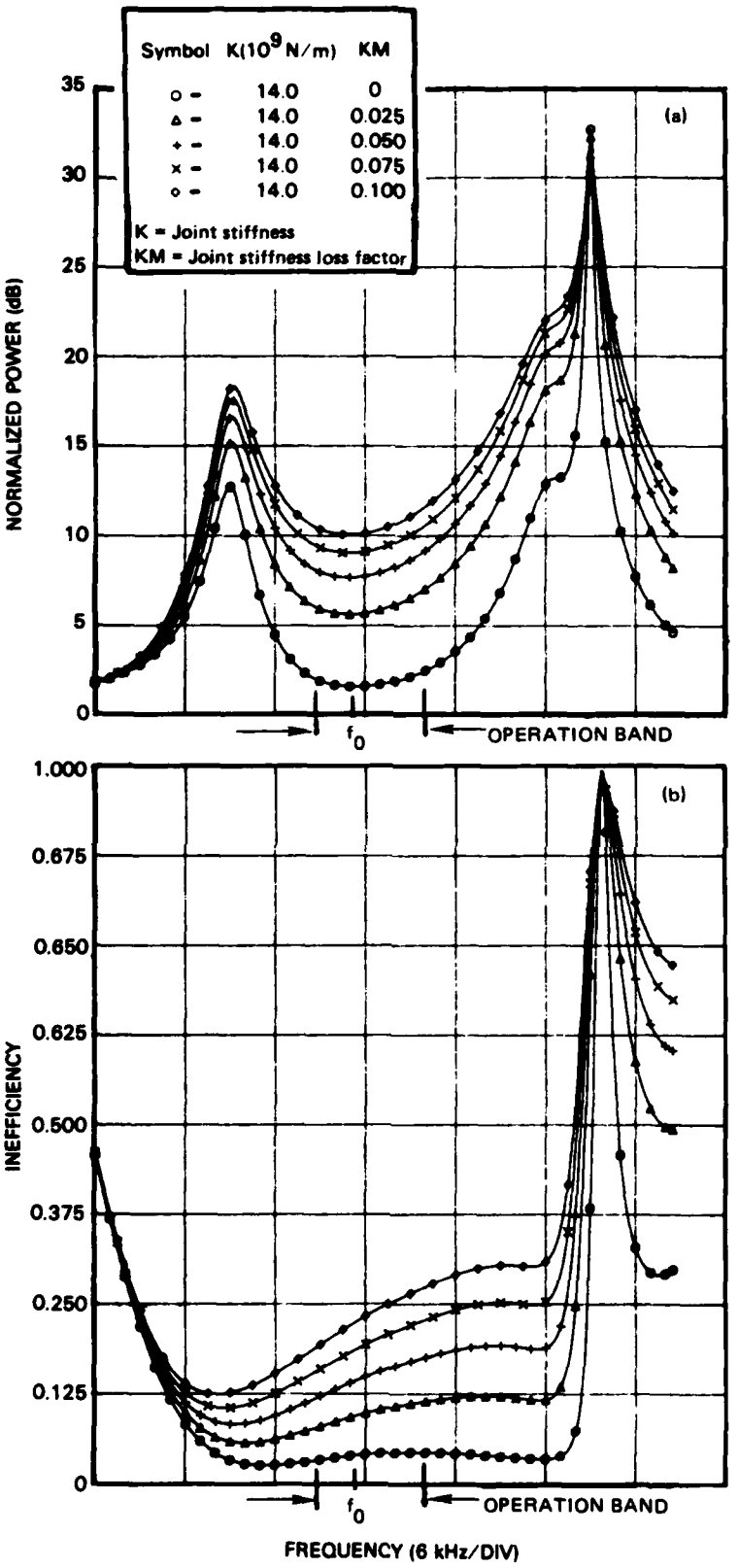

Figure 24. Modeled power dissipation and transducer inefficiency for a variation of joint loss factor in the ceramic-stack resonators.

5.0 CONCLUSIONS

5.1 SUMMARY OF THE CURRENT/THERMAL RUNAWAY PHENOMENON

The current/thermal runaway phenomenon observed recently in underwater transducers that incorporate ceramic-stack resonators is attributable to an insufficient final stress on one or more of the resonators in the transducer. This low stress was probably a result of a torque-wrench method of stressing the resonators. Seizure in the threads produced in several ways could result in low, erroneous stress biases. Stress relief due to thermal expansion may have also contributed to the problem. The cement/electrode joints are very temperature sensitive at low final stress biases. The cement and electrode both appear to be factors in that sensitivity, but the specifics of this behavior are not understood. Heating, in resonators with low final stress biases decreases the joint stiffness and perhaps increases the joint loss factor. The more compliant joints cause the impedance vs frequency responses to generally shift down in frequency. Because the operation band is centered about a point of maximum impedance (antiresonance) this shifting brings lower impedance regions into the operation band, causing the current to rise. The more compliant joints (and perhaps lossier joints) also cause more power to be dissipated in the resonator. The increased heating leads to further joint effects, which in turn cause further heating etc; current/thermal runaway results.

5.2 OTHER CONCLUSIONS

Other important conclusions from this study are:

1. Cement/electrode joints can cause serious problems in ceramic-stack resonators due to temperature-sensitive behavior. This sensitivity is mostly dependent on the amount of final stress applied (after cement curing). The sensitivity is drastic for resonators with low or no final stress. Resonators with a final stress of 2.8×10^7 Pa (4000 psi) yielded good temperature-insensitive performance, but those with a final stress of 6.9×10^6 Pa (1000 psi) demonstrated significant temperature-related performance degradation.

2. The temperature sensitivity involves a downward shift in frequency and flattening of the resonator's impedance vs frequency response as the temperature rises. The frequency shifting is due to joint compliance changes alone, specifically, the compliance increasing with increasing temperature. The flattening is due to increases in both the joint compliance and loss factor. In the band of operation, the antiresonance region, this results in a rise in the current amplitude (reduction in impedance) as well as an increase in the dissipated power as the temperature rises. The additional heating further changes the joint parameters, yielding further heating, etc. This process can result in current/thermal runaway.

3. For resonators that have low final stress biases, it is possible that stress relief occurs due to thermal expansion and causes degradation of the resonator's performance.

4. The application of a high final-stress bias, via a stress rod, eliminates the current/thermal runaway phenomenon that has been observed in transducers that employ ceramic-stack resonators. Resonators that do not contain stress rods are not likely to encounter significant self-heating because they are normally driven at low levels. Thus a high stress bias appears to be a sufficient cure for any temperature-related cement-joint problems presently known in Navy transducers.

6.0 RECOMMENDATIONS

Ceramic-stack resonators that are similar to those studied in this report and that may encounter elevated-temperature operational environments (>40°C) should be permanently restressed, after cement curing, to about 2.8×10^7 Pa (4000 psi). An equal stress should also be applied during cement curing in the assembly process as a safeguard in order to reduce the amount of cement in the resonator joints. These precautions will eliminate the possibility of current/thermal runaway or other performance degradation from temperature-sensitive behavior in the cement/electrode joints of the resonators.

There are two main items that may require further attention should some future need arise to better understand cement/electrode joints:

1. Regarding joint parameters, it may be necessary to give more attention to determining the absolute values of the joint parameters as a function of temperature, as opposed to relative changes (the focus in this report).

2. It may be necessary to examine the specifics of the behavior in the cement/electrode joints. The dependence of the behavior on the final stress bias is not presently understood and may be related to the individual behaviors of the cement and electrode.

APPENDIX

CERAMIC-RING PARAMETER MEASUREMENTS

The dumbbell method of determining joint parameters required that the ceramic parameters be known for the rings used in the dumbbells. The ceramic parameters of interest were the dielectric constant K_3^T and its loss tangent K_{3M}^T (also referred to by D or tan δ), the compliance s_{33}^D and its loss factor s_{33M}^D, and the piezoelectric constant g_{33} (the associated loss factor is negligible). The Ceramic parameter measurements were carried out by Martin Acoustic Software Technology (MAST). The approach used by MAST and the results are presented below.

APPROACH

For a long, thin piezoelectric ceramic bar there are well-known equations that relate ceramic parameters to experimental observables. The ceramic rings of concern in this report have appreciable cross-sectional area and thus the longitudinal characteristics differ from those of a long, thin bar. MAST used a finite-element model of a ceramic ring in order to determine an appropriate correction factor for each of the simple thin-bar equations.

Table A-1 presents the thin-bar equations and the correction factors determined by MAST. The measurables are C^T, D, Y_n, f_m and f_n. The product of the correction factor and the result of the thin-bar equation yields the corrected parameter value. Where ceramic parameters appear in the thin-bar equations (the g_{33} and S_{33M}^D equations) the uncorrected values are to be used. For example, in determining g_{33} the uncorrected values of S_{33M}^D and k_{33} are to be used in the thin-bar equation and then the correction factor applied.

The correction factors for g_{33} and S_{33M}^D simply result from propagating the k_{33} and S_{33}^D corrections through the g_{33} and S_{33M}^D equations. The correction factors shown in Table A-1 for these two parameters are approximate, corresponding to an average uncorrected k_{33} of 0.6. As can be seen from the equations the exact correction factor depends on the value of k_{33}. Table A-2 shows how to compute the exact correction factors for g_{33} and S_{33M}^D.

Thin-Bar Equation	Multiplicative Correction Factor
$K_3^T = \frac{C^T L}{\varepsilon_o A}$	None
$s_{33}^D = \frac{1}{4\rho f_n^2 L^2}$	0.9939
$k_{33} = (x/\tan x)^{1/2};\ x = \frac{\pi}{2}\ \frac{f_m}{f_n}$	1.0902
$g_{33} = \left(\frac{s_{33}^D\ k_{33}^2}{(1-k_{33}^2)\ \varepsilon_o K_3^T}\right)^{1/2}$	1.15[a]
$K_{3M}^T \equiv D \equiv \tan \delta$	None
$s_{33M}^D = \frac{2}{\pi 3}\ \frac{k_{33}^2}{1-k_{33}^2}\ \frac{\lvert Y_n \rvert}{f_n C^T}$	1.32[a]

C^T ≡ free capacitance at 1 kHz

A ≡ area of ceramic ring face

L ≡ length (face-to-face) of ceramic ring

ε_o ≡ dielectric constant of free space

ρ ≡ density of ceramic

D ≡ dielectric dissipation at 1 kHz

Y_n ≡ minimum electrical admittance magnitude

f_m ≡ frequency at maximum electrical admittance magnitude

f_n ≡ frequency at minimum electrical admittance magnitude

a Corresponds to an uncorrected k_{33} of 0.6.

Table A-1. Thin-bar equations and correction factors for actual ceramic ring.

Parameter	Multiplicative Correction Factor
g_{33}	$1.0868\left(\frac{1-k_{33}^2}{1-1.1885k_{33}^2}\right)^{1/2}$
s_{33M}^D	$1.1885\ \frac{1-k_{33}^2}{1-1.1885k_{33}^2}$

Table A-2. Exact correction factors for g_{33} and s_{33}^D.

The procedure for the determination of the temperature dependence of ceramic parameters was as follows. The ceramic rings were placed in the oven and measurements of C^T, D, Y_n, f_m and f_n were taken at a room temperature of approximately 21°C (70°F). The oven controls were set at 46°C (115°F) and within 5 minutes the oven was at the specified temperature. One hour later, measurements were made at the higher temperature. The process continued using 25°C increments to achieve temperatures of 21, 46, 71, 96, and 121°C.

The temperature history of the ceramic rings is a matter of importance. Measurements generally were made first on rings that had not been out of an ordinary (room temperature) environment since being polarized long ago. After each set of temperature-cycled measurements, the units were allowed to stabilize at room temperature. They were then exposed to a temperature soaking of 2-1/2 hours at 66°C (150°F). After about one week at room temperature, another measurement cycle began. Although 14 rings were put through the first measurement heat cycle, only six were carried through three more heat cycle measurements and then used in the construction of the three dumbbells. The histories of these six ceramic rings are given in Table A-3.

RESULTS

Figures A-1 through A-6 present the results of the ceramic parameter determinations for the six rings. Each figure applies to a single ring and shows the temperature dependence of ceramic parameters of each of the four

CERAMIC RING ID	Cure Heat Cycle 1 (2.5 hrs @ 66°C)	Meas. Heat Cycle 1 (21-121°C)	Cure Heat Cycle 2 (2.5 hrs @ 66°C)	Meas. Heat Cycle 2 (21-121°C)	Cure Heat Cycle 3 (2.5 hrs @ 66°C)	Meas. Heat Cycle 3 (21-121°C)	Cure Heat Cycle 4 (2.5 hrs @ 66°C)	Meas. Heat Cycle 4 (21-121°C)
33	4-28-82	5-5-82	5-21-82	6-1-82	6-10-82	6-23-82	7-6-82	7-22-82
36	5-4-82	5-12-82	5-21-82	6-1-82	6-10-82	6-23-82	7-6-82	7-22-82
37	"	5-12-82	5-21-82	6-1-82	6-10-82	6-23-82	7-6-82	7-22-82
40	"	5-17-82	5-21-82	6-8-82	6-17-82	6-24-82	7-6-82	7-26-82
44	"	5-10-82	5-21-82	6-8-82	6-17-82	6-24-82	7-6-82	7-26-82
49	"	5-10-82	5-26-82	6-4-82	6-17-82	6-24-82	7-6-82	7-26-82

Table A-3. Processing of piezoelectric ceramic rings.

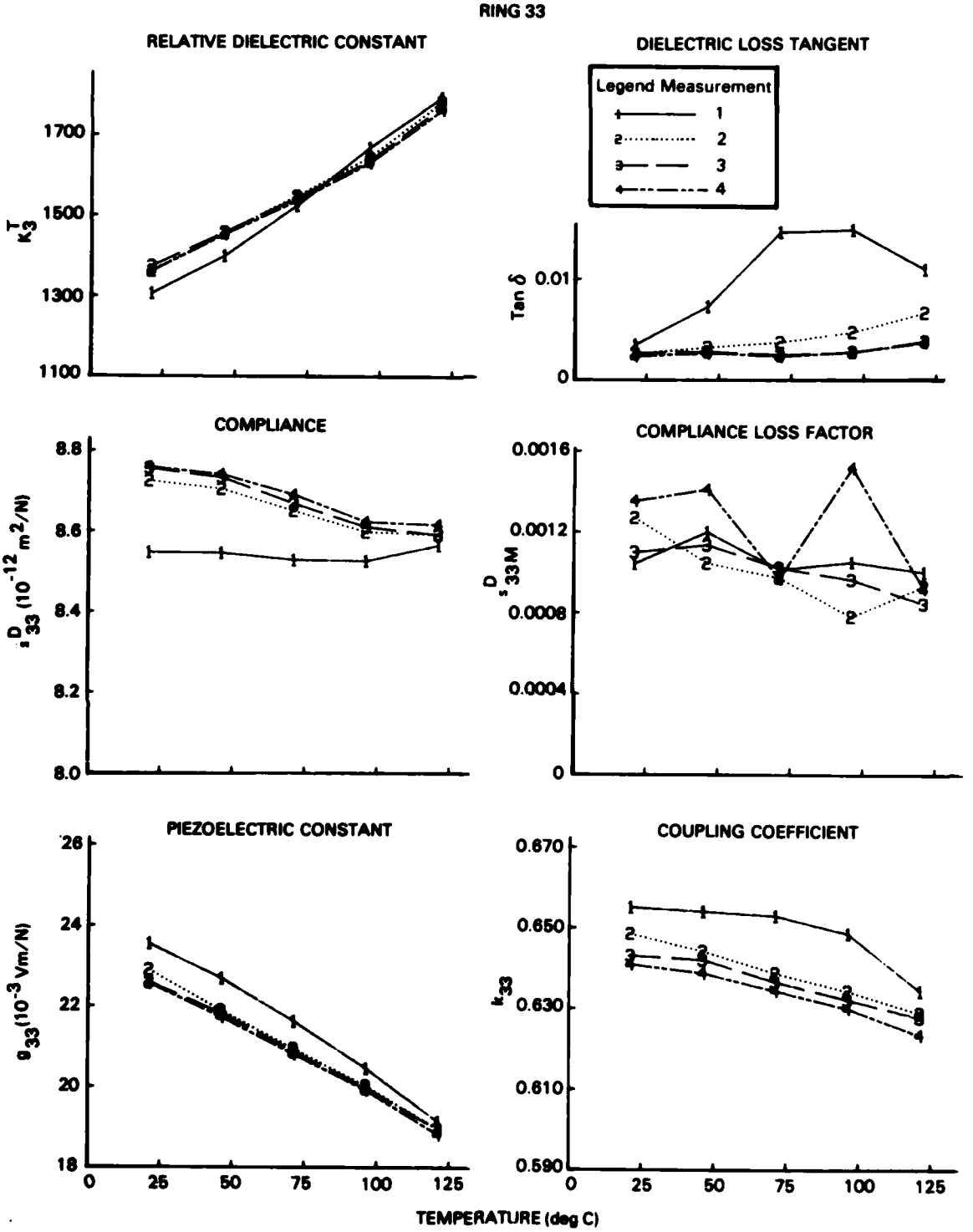

Figure A-1. Four successive heat cycle measurements of the ceramic parameters for ceramic ring 33.

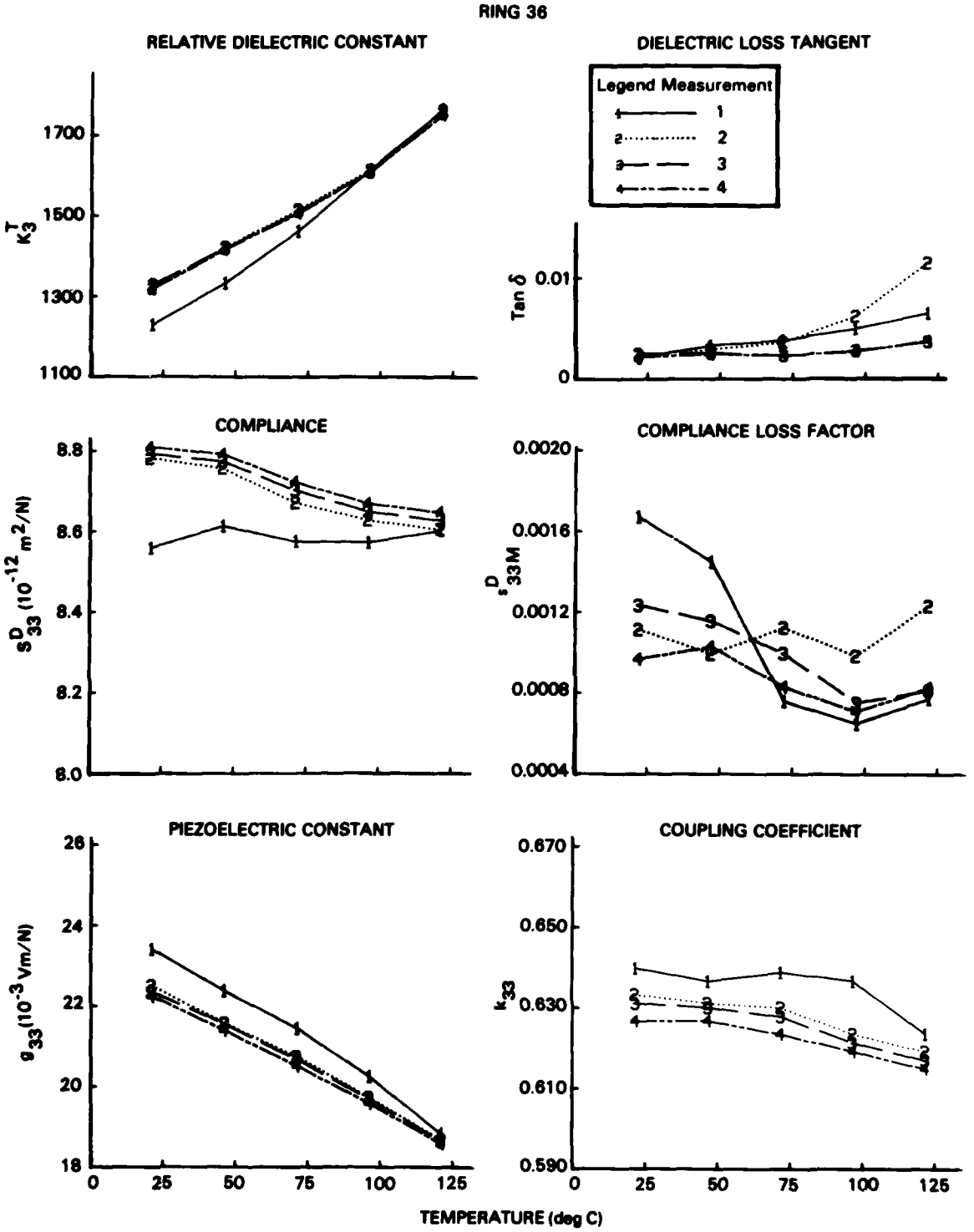

Figure A-2. Four successive heat cycle measurements of the ceramic parameters for ceramic ring 36.

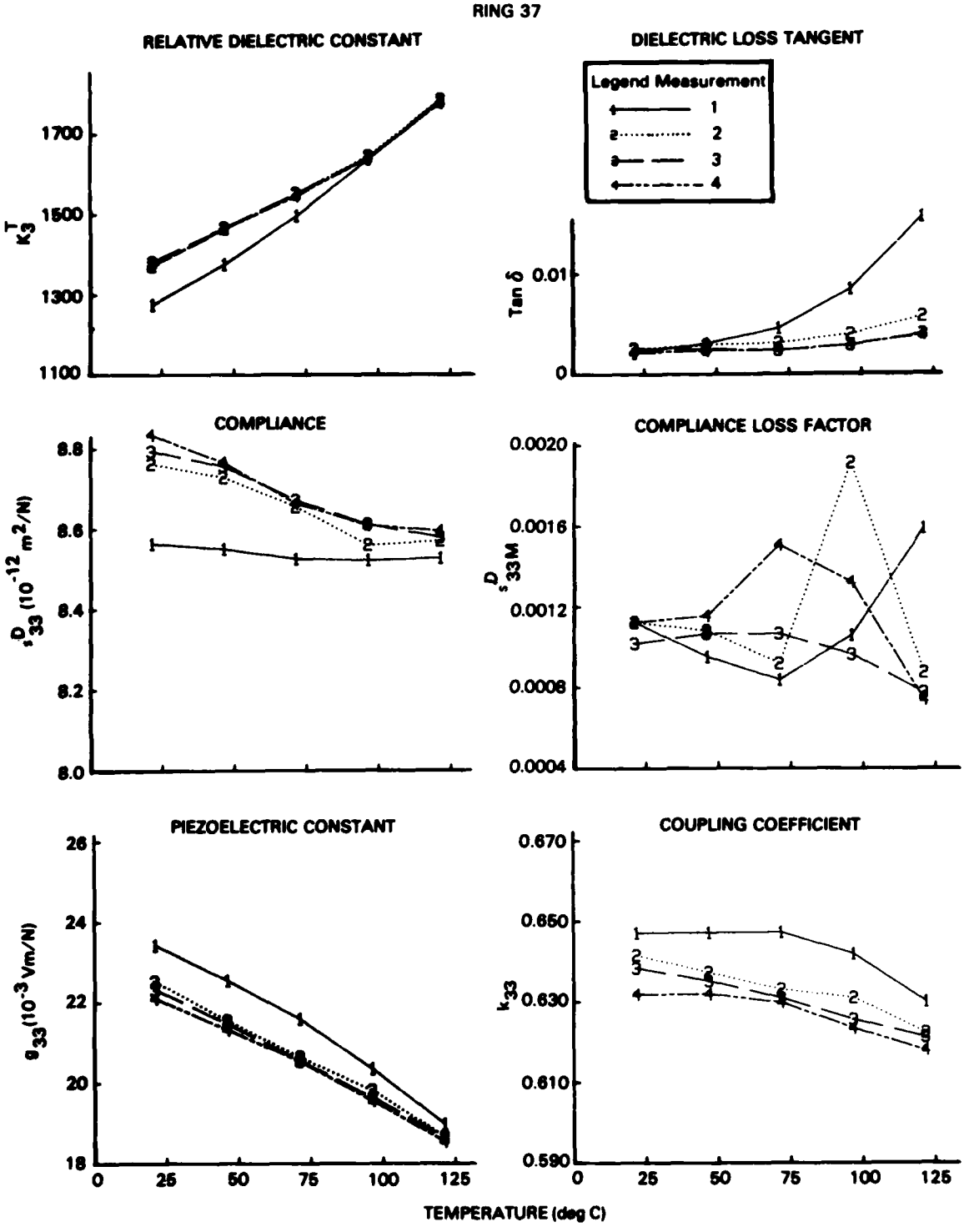

Figure A-3. Four successive heat cycle measurements of the ceramic parameters for ceramic ring 37.

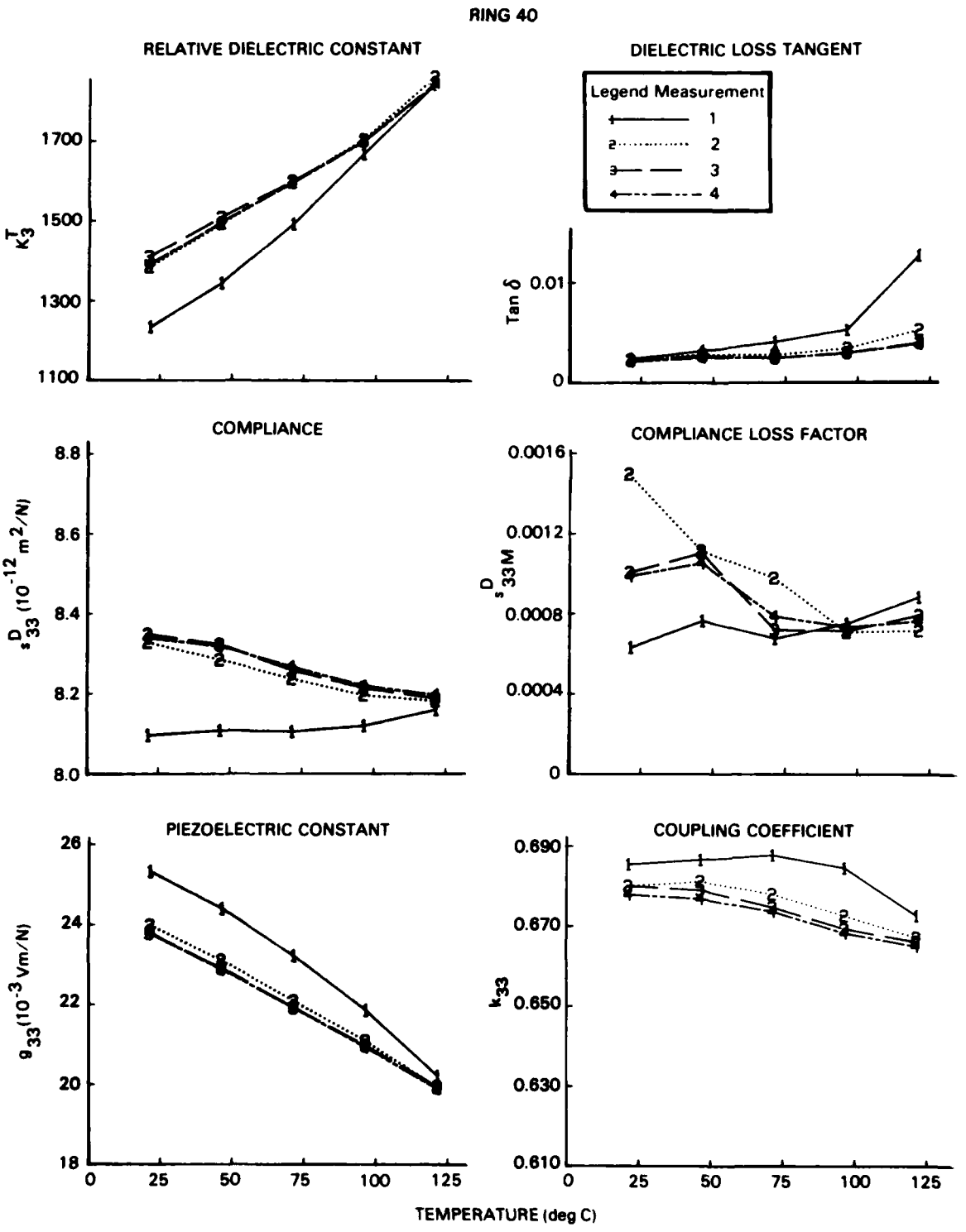

Figure A-4. Four successive heat cycle measurements of the ceramic parameters for ceramic ring 40.

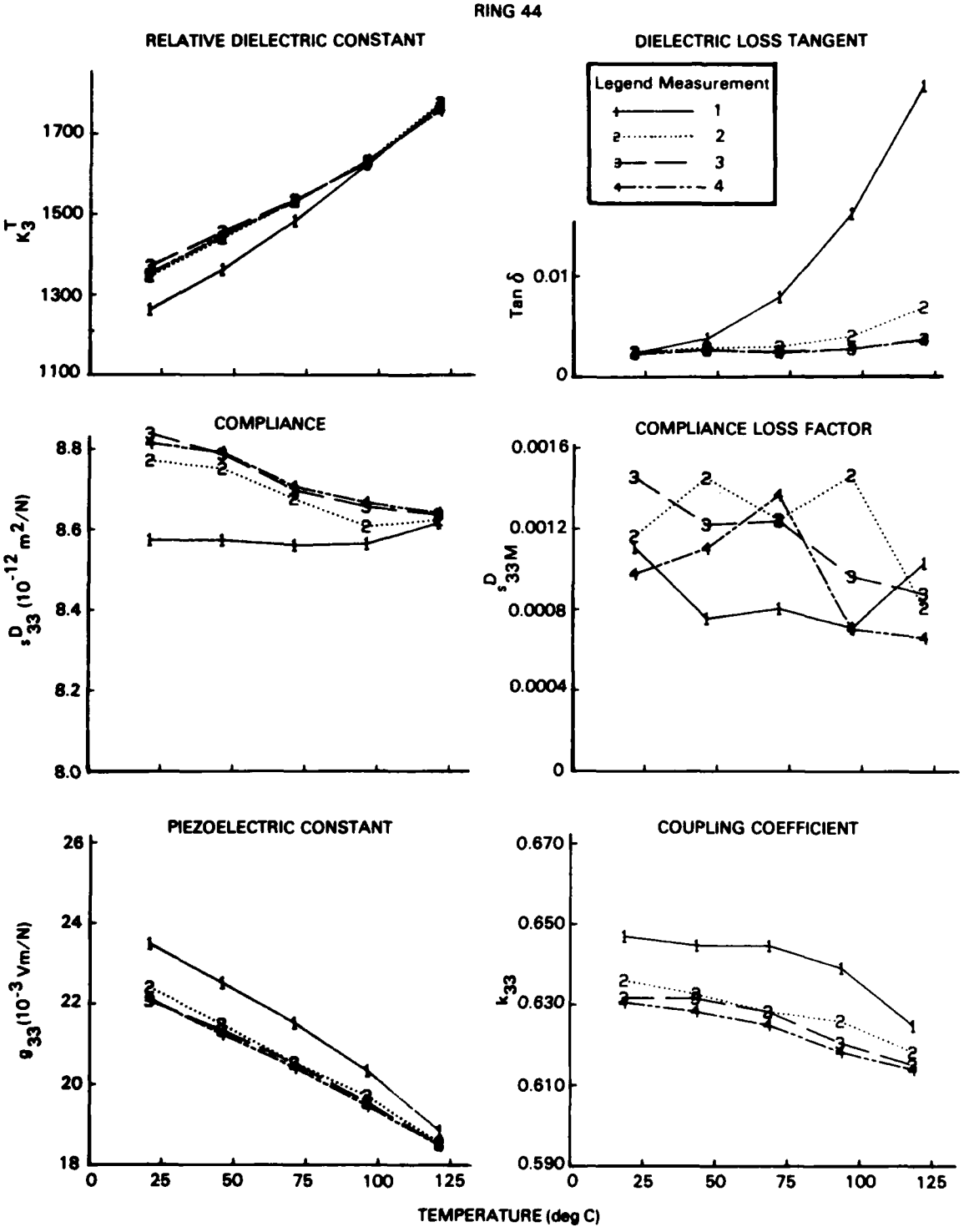

Figure A-5. Four successive heat cycle measurements of the ceramic parameters for ceramic ring 44.

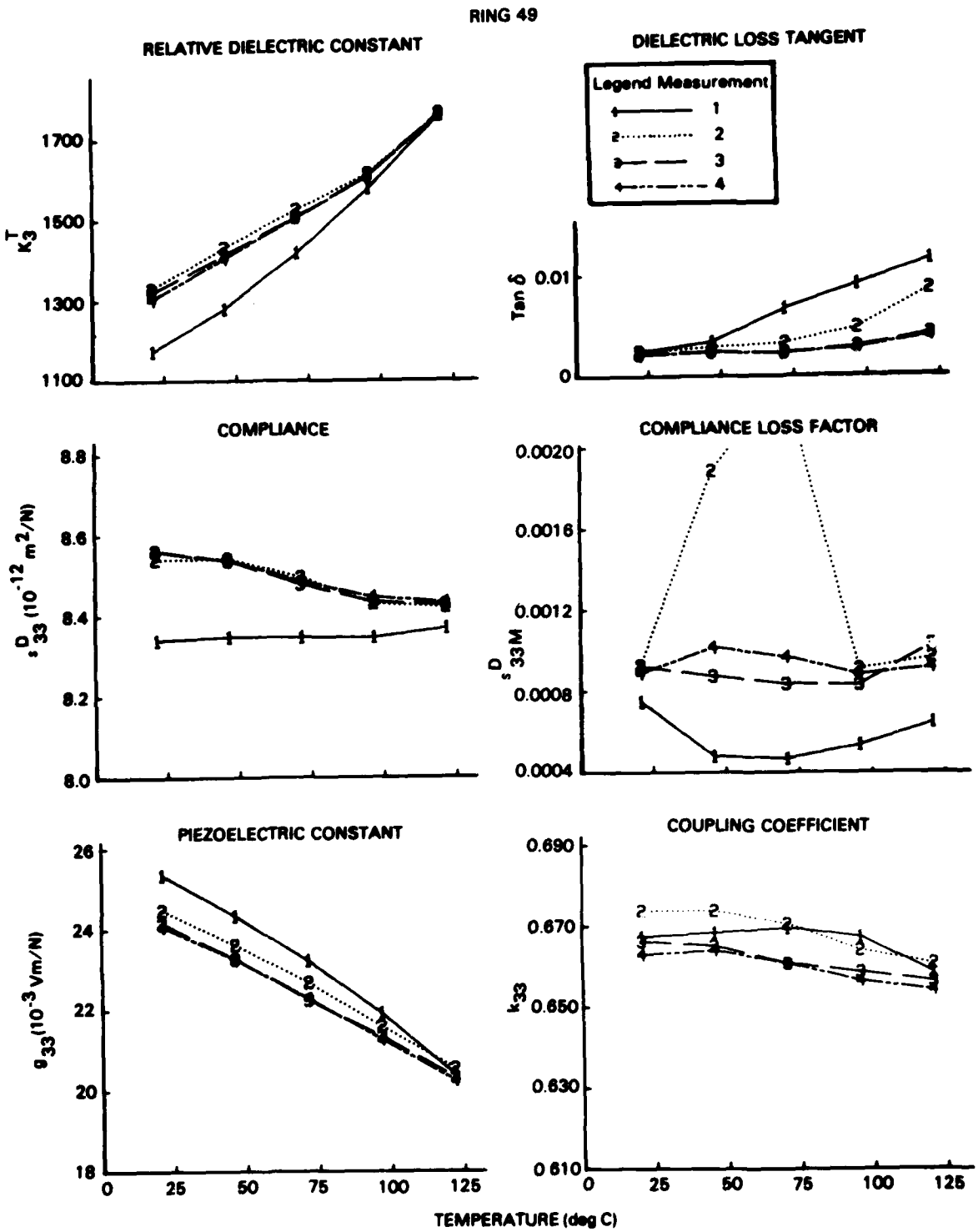

Figure A-6. Four successive heat cycle measurements of the ceramic parameters for ceramic ring 49.

heat cycle measurements. The ceramic parameters shown are the relative dielectric constant (K_3^T), the dielectric loss tangent (tan δ), the mechanical compliance (s_{33}^D) and its loss factor (s_{33M}^D), the piezoelectric constant (g_{33}), and the coupling factor (k_{33}). In the first two heat cycle measurements a fixture problem resulted in an erroneously high measurement of the dissipation factor. The problem was corrected and the results for the last two cycles are correct.

Study of Figures A-1 through A-6 leads to the following observations:

1. In the first heat cycle measurement the elastic parameter, s_{33}^D, is nearly constant with a slight increase above 100°C. During the next three heat cycle measurements s_{33}^D is higher and decreases as the temperature rises.

2. During all heat cycles the piezoelectric constant, g_{33}, changes much more than do s_{33}^D and k_{33}, but less than does K_3^T. In addition K_3^T increases more during the first heat cycle measurement than it does in the successive cycles. At 121°C K_3^T is nearly the same for all heat cycles but at room temperature is is less during the first heat cycle measurement.

3. During the first heat cycle measurement k_{33} is mostly constant to 75°C but then decreases. During the successive heat cycle measurement k_{33} begins to decrease as soon as the temperature exceeds about 50°C.

4. The piezoelectric constant, g_{33}, is strongly affected by temperature. As the equation for g_{33}, in Table A-1, shows, each of the parameters varies to make g_{33} drop as the temperature increases. Specifically, K_3^T increases, where as s_{33}^D and k_{33} decrease. Pronounced decreases of g_{33} with rising temperature are evident for all six rings in the figures. In addition, the piezoelectric activity is observed to decrease as a function of heat cycle.

These observations cause one to question the value of 100°C heat soak of ceramic materials, as is often done in order to stabilize behavior. In fact, the elastic constant is relatively independent of temperature for the first heat cycle but not afterward. The coupling coefficient is decreased after the first cycle and the temperature dependence is generally more severe. Aging characteristics were not measured, and aging may be reduced by such a heat

soak. However, the temperature dependence was degraded during the experiments reported here. At best the issue of a heat soak is a design tradeoff consideration for a source transducer that will be driven to moderately high fields.

The pertinence of the results in Figures A-1 through A-6 to the cement joint investigation can be summarized as follows. Note that the temperature behaviors of K_3^T, s_{33}^D, g_{33}, tan δ and k_{33} are nearly the same for heat cycles two, three, and four. The difference between heat cycle one and the rest results from the exposure of the ceramic rings to the high temperature of 121°C during the first cycle. Although all of the rings had been "heat soaked" (in the heat cure cycle) prior to the measurements, the soak temperature was only 66°C, significantly less than the maximum measurement temperature of 121°C. The major conclusion that is relevant to the effort to measure cement-joint parameters is that after the first heat cycle measurement, the ceramic parameters remain fairly constant between successive heat cycle measurements. This means that the ceramic parameters of rings that are cemented into a dumbbell are not affected much by the cement heat cure and ensuing heat cycle measurement that is required for the cement-joint parameter determination, as long as the rings were previously exposed to at least one heat cycle measurement. That feature provided confidence that once ceramic parameters were measured in a heat cycle, they were still valid when the ceramic rings were subsequently cemented together and subjected to a cure cycle and a measurement heat cycle.

END

FILMED

02 — 84

DTIC